

Nuclear Magnetic Resonance for Studies of Carbon Nanostructures

Alexander M. Panich

*Department of Physics, Ben-Gurion University of the Negev,
Be'er Sheva, Israel*

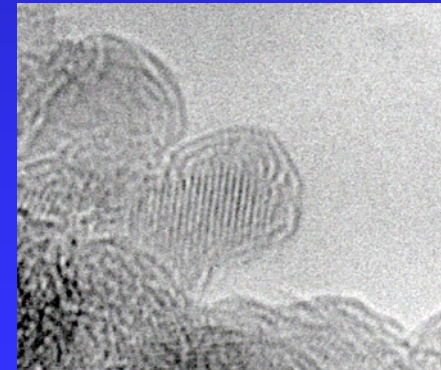
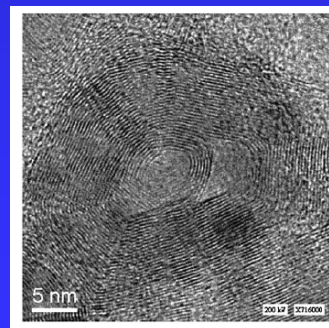
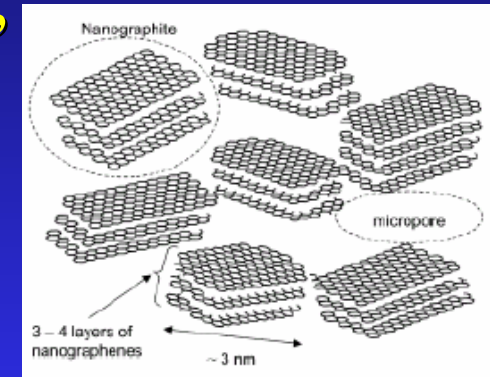
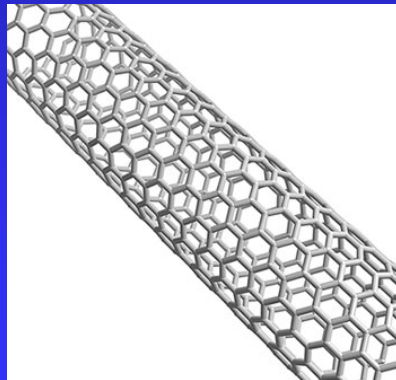
Joint International Conference “Advanced Carbon Nanostructures”
International school for young scientists "Carbon Nanostructures Diagnostics"
September 6, 2011, St. Petersburg, Russia

Outline:

1. Introduction to Nuclear Magnetic Resonance (NMR).

2. NMR studies of carbon nanomaterials:

pure and doped fullerenes,
carbon nanotubes,
nanofraphite,
carbon onions,
nanodiamonds

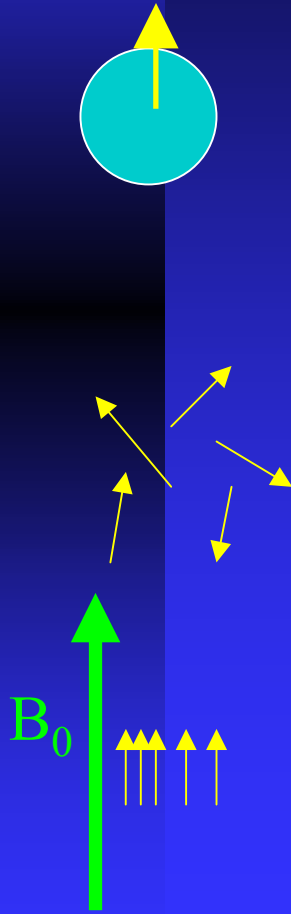


Nuclear Magnetic Resonance (NMR):

- (a) physical phenomenon
and
- (b) method of investigation
which is used
in physics, chemistry, biology,
medicine (MRI)
and materials science

1. Nuclear Magnetic Resonance (NMR) for 15 minutes

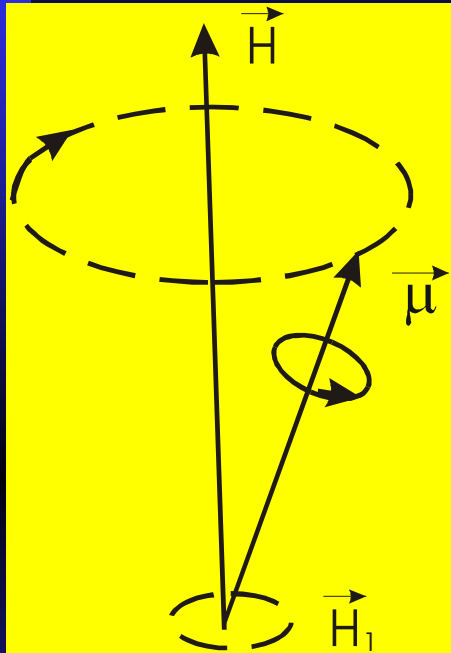
All nuclei with odd mass number have an intrinsic angular momentum and magnetic moment, in other words a spin $I > 0$, which comes in multiples of $\frac{1}{2}$. Nuclei with even mass number have spin 0, 1, 2, 3 etc.



$B_0 = 0$ – random orientations of spins.

In applied magnetic field B_0 , spin will stay along the field direction, as a magnetic needle in compass.

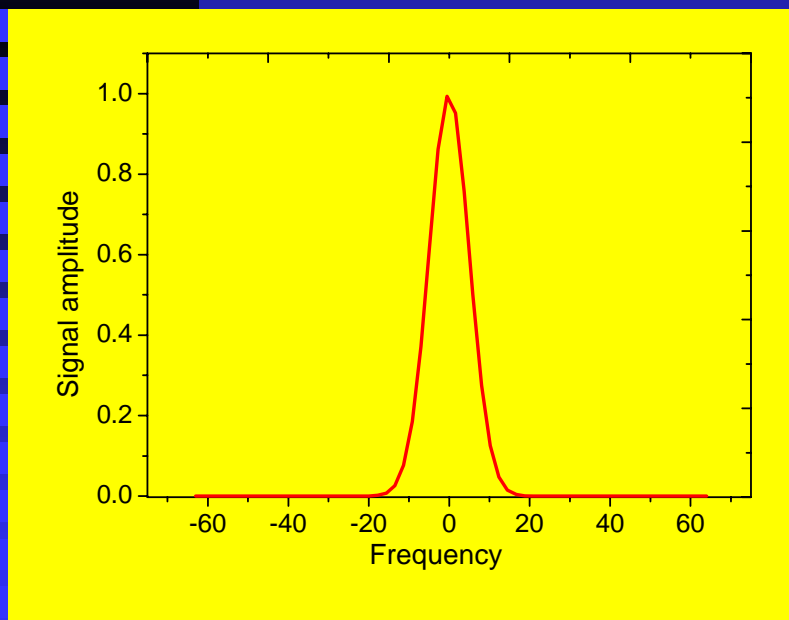
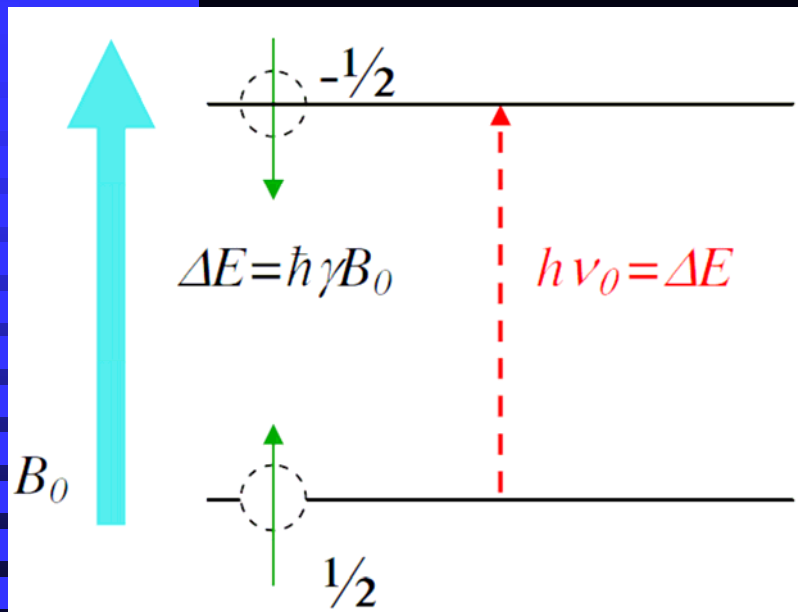
Precession of nuclear magnetic moment



Nuclear magnetic moment tilted from the direction of the applied magnetic field B_0 undergoes a precession around B_0 with the frequency

$$\nu_0 = \gamma B_0 / 2\pi$$

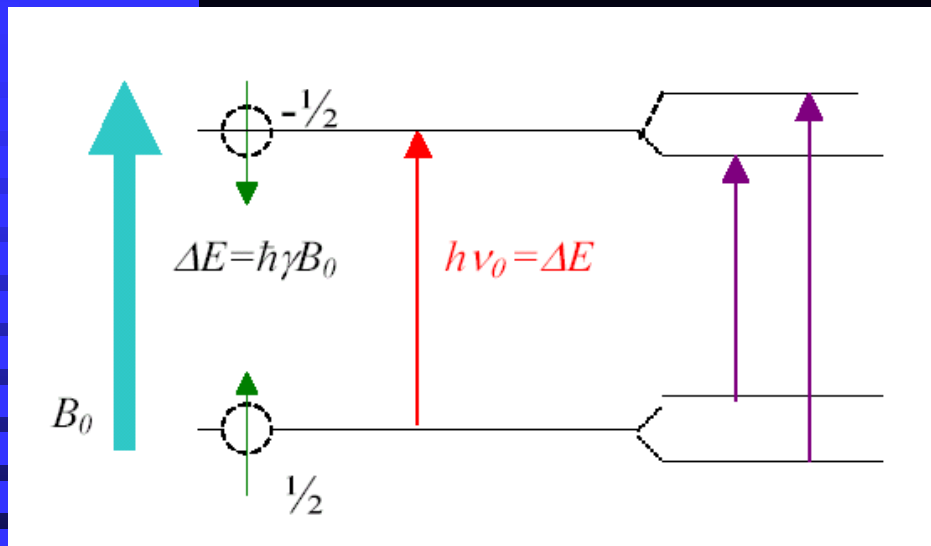
(Larmor frequency).



In magnetic field B_0 , nuclear spin $\frac{1}{2}$ exhibits two energy levels, corresponding to “up” and “down” spin orientations. Splitting is proportional to applied magnetic field.

Oscillating electromagnetic field of frequency ν , such as $h\nu = \Delta E$, gives rise to the resonance transition between the energy levels that is NMR.

Different nuclei have different γ and different resonance frequencies.



Real systems: energy levels are shifted, split or spread due to interactions of nuclear spin with other nuclear spins and electron spins, which depend on the distance between spins, electron cloud overlap, etc.

We measure these interactions and receive information about crystal and electronic structure, phase transitions, internal motions, etc. at the atomic level.

Nuclear spin is a probe that is naturally embodied into the crystal lattice and 'sees' all what happens in this lattice.

$$\mathcal{H} = \mathcal{H}_z + \mathcal{H}_{dip} + \mathcal{H}_j + \mathcal{H}_Q + \mathcal{H}_{cs} + \mathcal{H}_{hf}$$

$$\mathcal{H}_z = -\gamma_n \hbar B_0 I_z$$

Zeeman term

$$\mathcal{H}_{dip} = b_{ij} [I_{zi} I_{zj} - (I_i^+ I_j + I_i I_j^+)/4]$$

*nuclear dipole-dipole coupling
where $b_{ij} = h\gamma_n^2 (3\cos^2\theta - 1)/r_{ij}^3$*

$$\mathcal{H}_j = h J \cdot I_i \cdot I_j$$

indirect nuclear exchange coupling

$$\mathcal{H}_Q = [e^2 q Q / 4I(2I-1)] \times [3I_z^2 - I(I+1)]$$

quadrupole interaction of nuclear quadrupole moment Q with electric field gradient q

$$\mathcal{H}_{cs} = \gamma_n I \cdot \sigma B_0$$

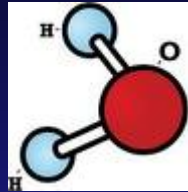
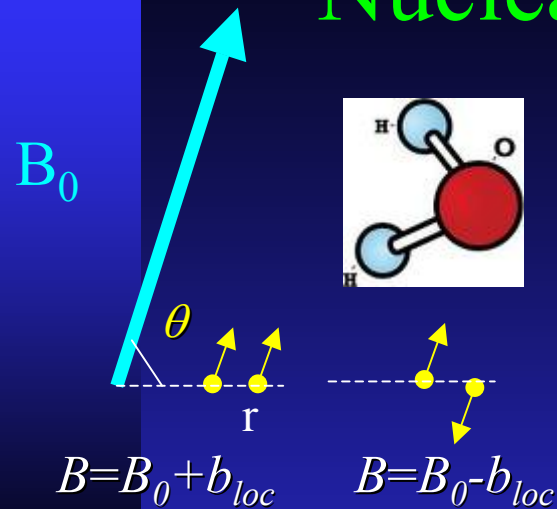
chemical shift (weak field at nucleus site induced by circulating electrons)

$$\mathcal{H}_{hf} = h I \cdot A \cdot S, \quad A \sim \gamma_n h \mu_B |\Psi(0)|^2$$

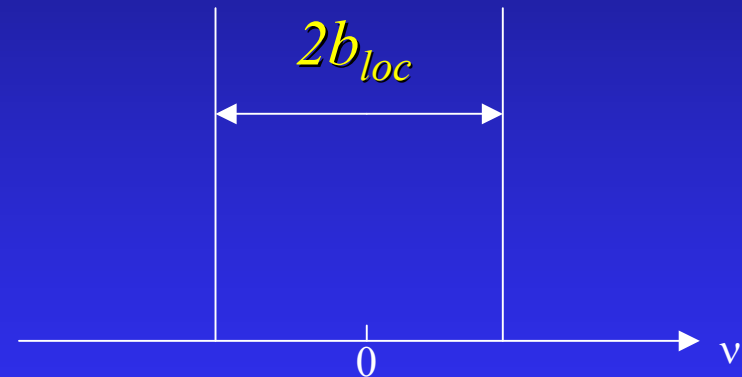
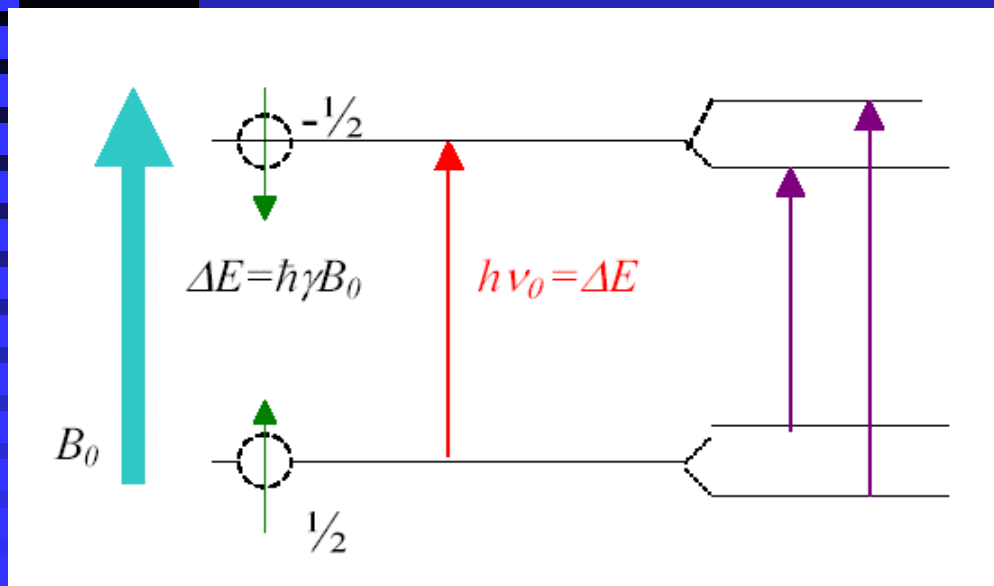
hyperfine/contact coupling of nuclear spin I with spins S of conduction or localized unpaired electrons

Luckily, very often one of these interaction dominates and allows us to study it.

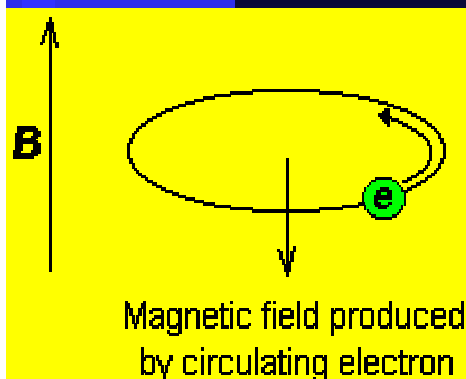
Nuclear dipole-dipole interaction



Two spins interact with each other:
 $B = B_0 \pm b_{loc}$, $b_{loc} = \mu(3\cos^2\theta - 1)/r^3$
 + or - as the partner spin is parallel or antiparallel to B_0

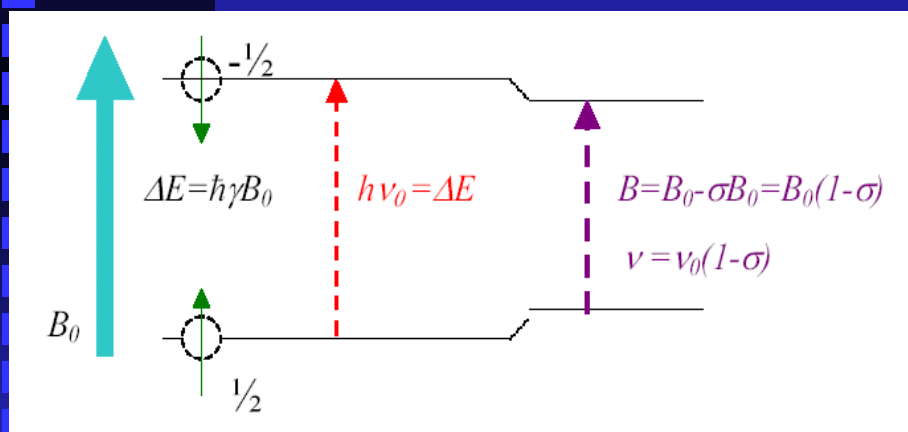


Chemical shift and inequivalent atoms



In NMR experiment, actual field at nucleus is the sum of a strong applied magnetic field B_0 and a weak field induced by electrons circulating around nucleus:

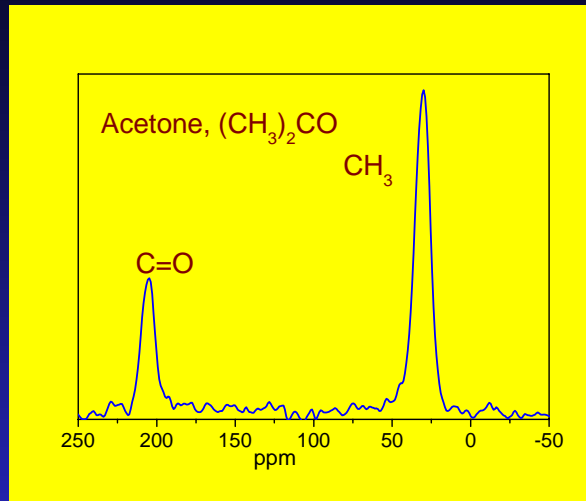
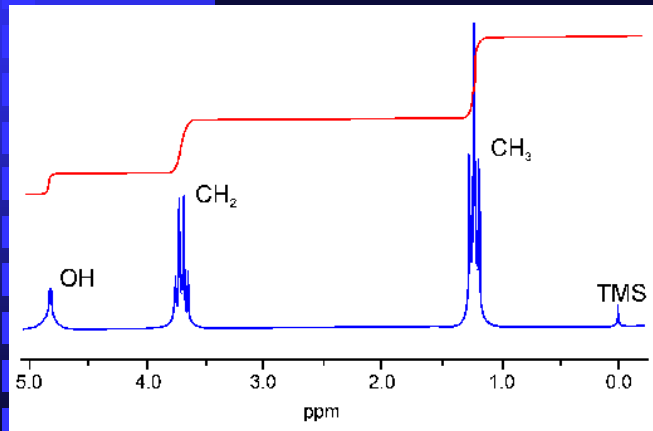
$$\nu_0 = \gamma B_0; \quad B = B_0 - b_{cs} = B_0(1 - b_{cs}/B_0) = B_0(1 - \sigma)$$



It yields a deviation of the NMR frequency from ν_0 . This deviation σ , called chemical shift/shielding.

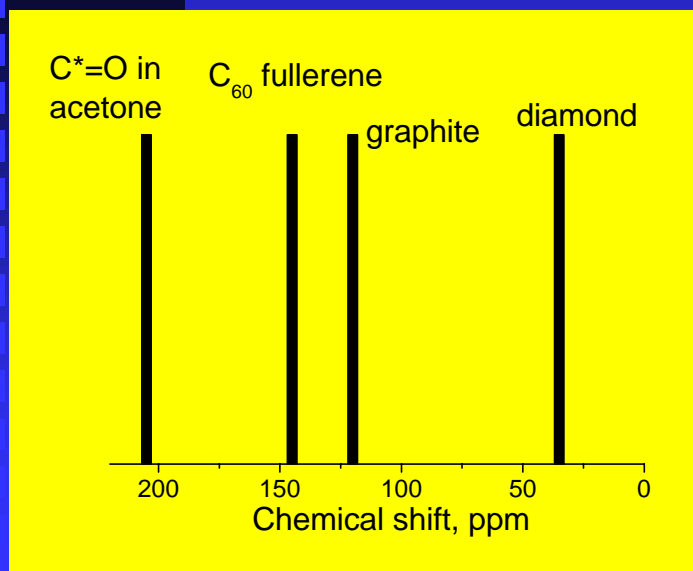
Different electron environments at different chemical bonds cause different CS, which allows to distinguish inequivalent carbon atoms in the lattice/molecule one from another.

Chemical shift and inequivalent atoms - 2



Chemical shift is sensitive to the nature of chemical bond and varies from one compound to another. One can determine what compound he measures according to the CS of NMR spectrum.

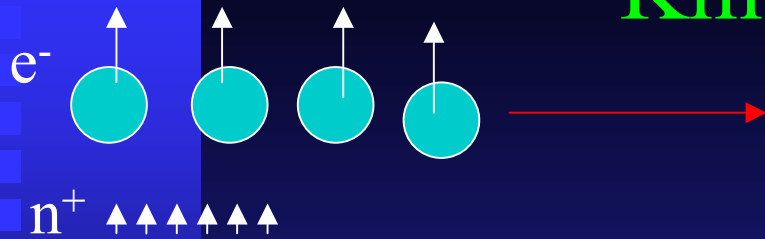
NMR spectrum of ethanol
CH₃-CH₂-OH



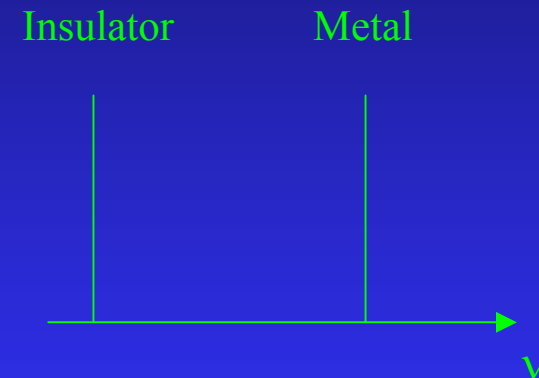
Chemical shifts are defined in ppm (part per million), in values that are independent on the magnetic field strength; $1 \text{ ppm} = \frac{\Delta\nu}{\nu_0} \times 10^6$

The higher the applied magnetic field, the better the spectral resolution.

Knight shift in conductors

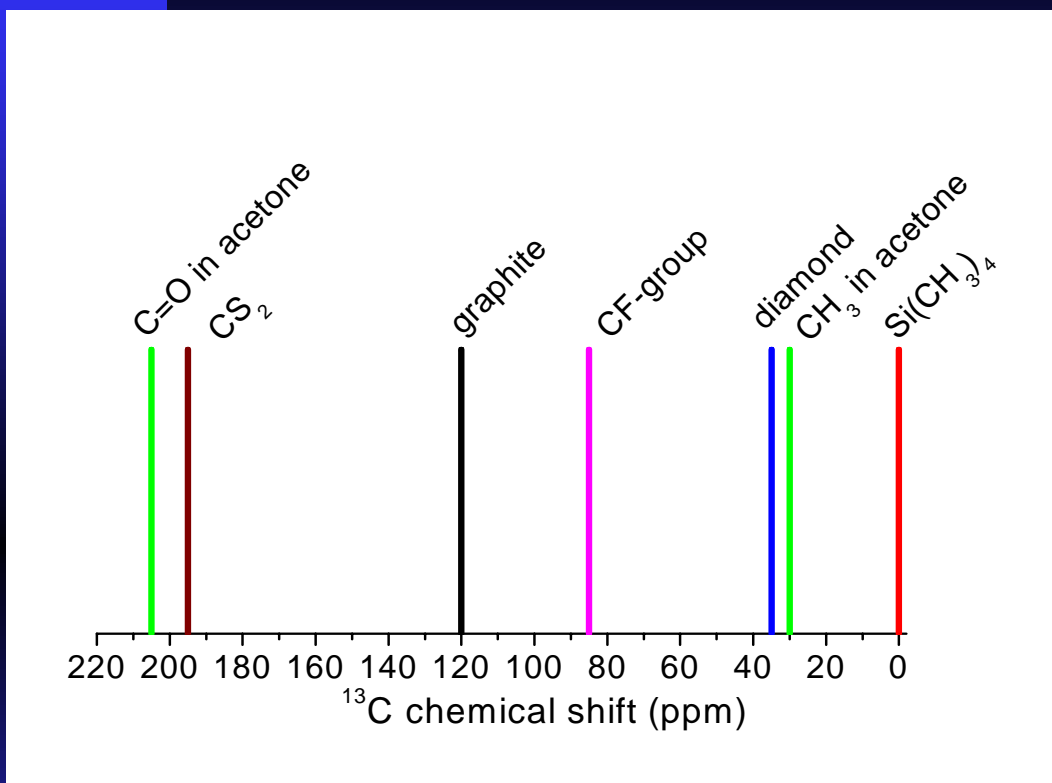


- Knight shift is characteristic of conductors.
- It originates from the hyperfine interaction between nuclear spins and spins of conduction electrons and is produced by electronic s states having a nonzero value $|\psi(0)|^2$ at the nucleus site.
- Study of electronic structure of conductors.



$$K \sim \langle |\psi(0)|^2 \rangle_{E_F} \rho(E_F)$$

Chemical shielding tensor



Sketch of carbon chemical shift (CS) scale.

CS are defined in ppm, in values that are independent on field strength.

$$\sigma [\text{ppm}] = (\Delta\nu/\nu_0) \times 10^6.$$

Centers of gravity of NMR lines are shown.

However, since electron clouds are generally non-spherical, CS is not a scalar but the second rank tensor.

$$\begin{pmatrix} \sigma_{11} & 0 & 0 \\ 0 & \sigma_{22} & 0 \\ 0 & 0 & \sigma_{33} \end{pmatrix}$$

Matrix of
non-axially symmetric second rank tensor

$$\begin{pmatrix} \sigma_{\perp} & 0 & 0 \\ 0 & \sigma_{\perp} & 0 \\ 0 & 0 & \sigma_{\parallel} \end{pmatrix}$$

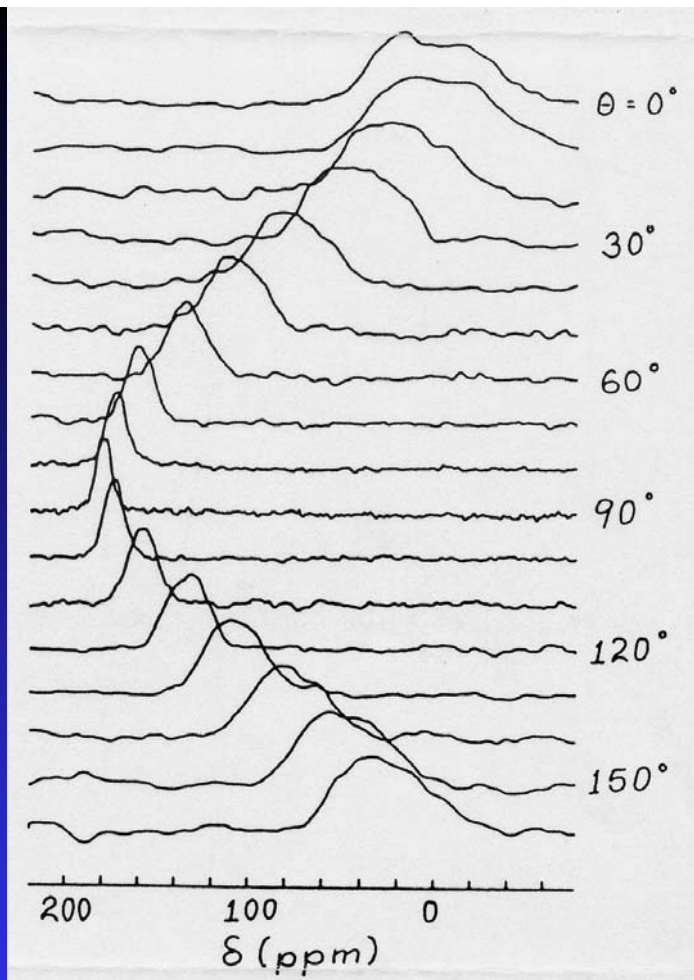
Matrix of
axially symmetric second rank tensor

$$\sigma_{11} = \sigma_{22} = \sigma_{\perp}, \quad \sigma_{33} = \sigma_{\parallel}$$

The line position in single crystal is angular dependent. For axially symmetric tensor, the chemical shift is given as

$$\sigma = \sigma_{iso} + A(3\cos^2\alpha - 1),$$

where $A = (\sigma_{\parallel} - \sigma_{\perp})/3$ and $\alpha(B_0, z)$ is the angle between the applied magnetic field B_0 and the principal axis of the tensor.



Angular dependence of ^{13}C NMR spectra in HOPG (H. A. Resing *et al*, 1985)

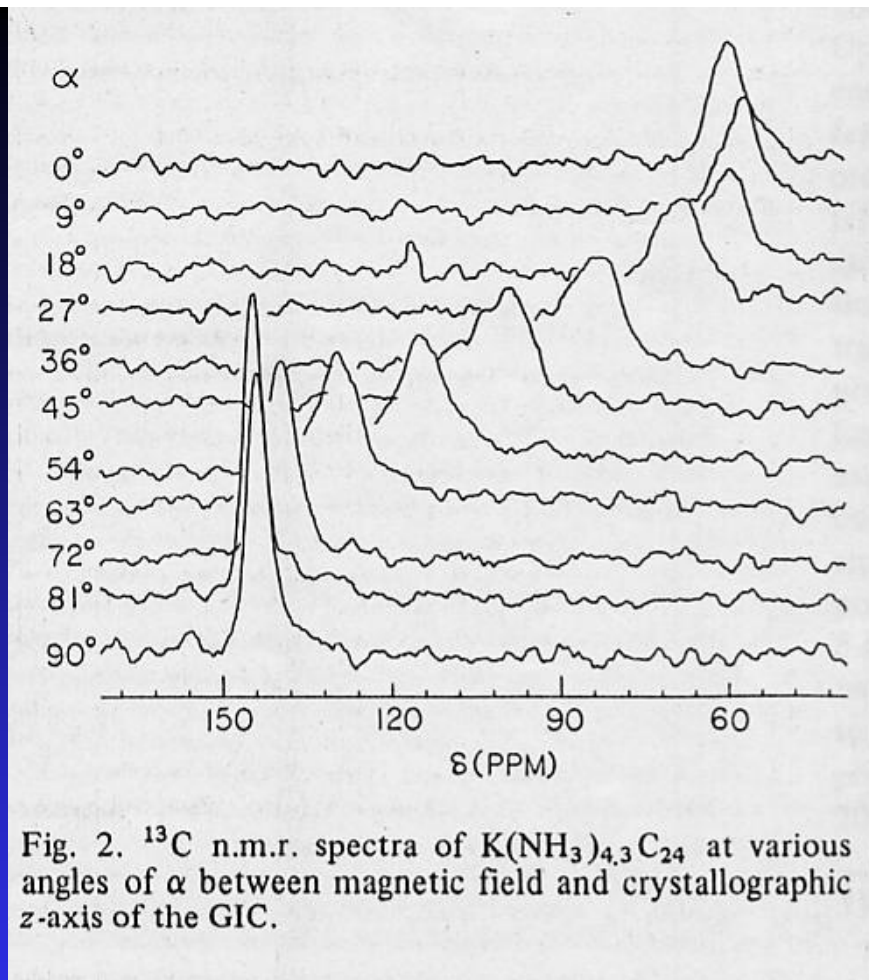
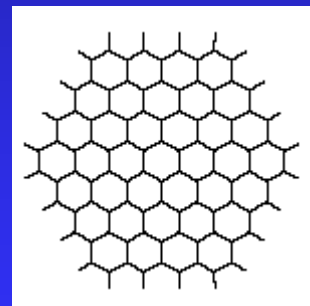
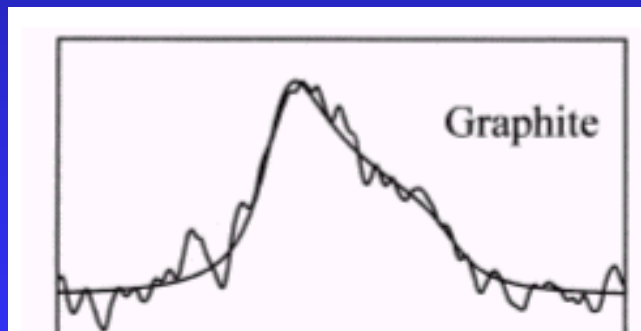
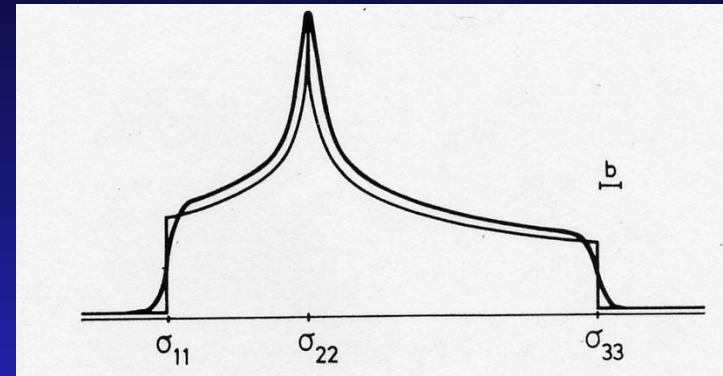
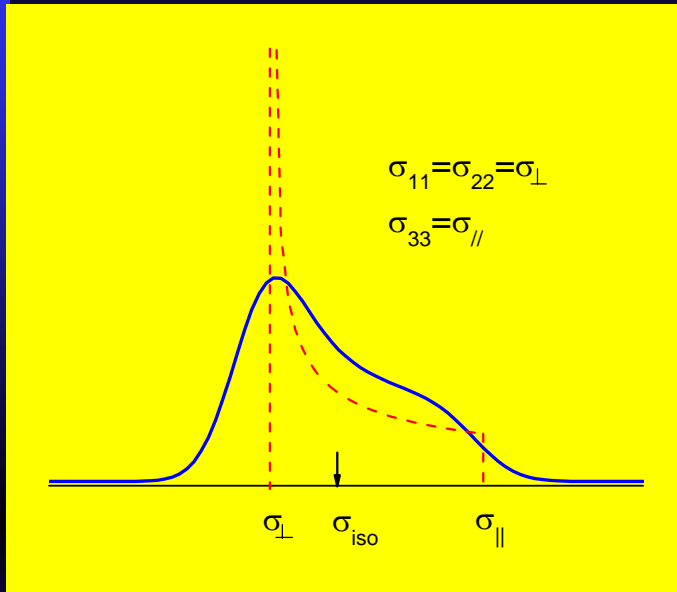


Fig. 2. ^{13}C n.m.r. spectra of $\text{K}(\text{NH}_3)_{4.3}\text{C}_{24}$ at various angles of α between magnetic field and crystallographic z-axis of the GIC.

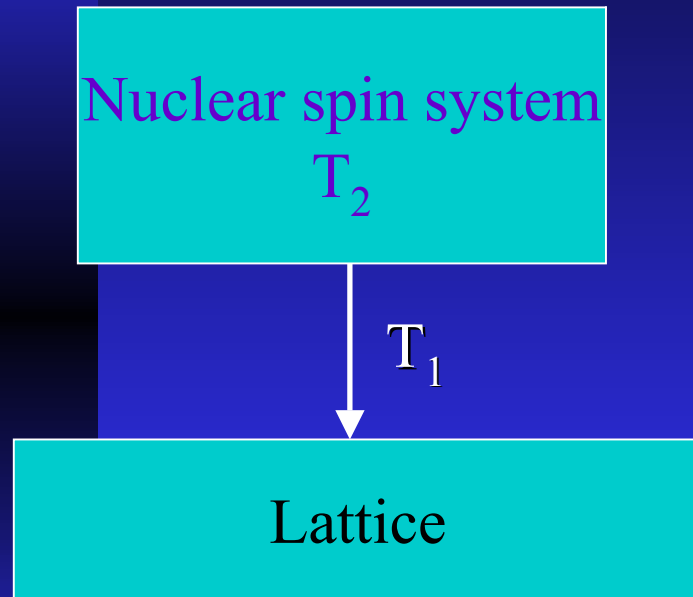
(T. Tsang, R. M. Fronko, H. A. Resing *et al*, *Solid State Commun.* 62, 117, 1987)

Powder sample yields a superposition of spectra at all possible orientations. Characteristic line shapes for axially and non-axially symmetric shielding tensors:



(H. Darmstadt, C. Roy, et al., Carbon 20, 1279, 2000).

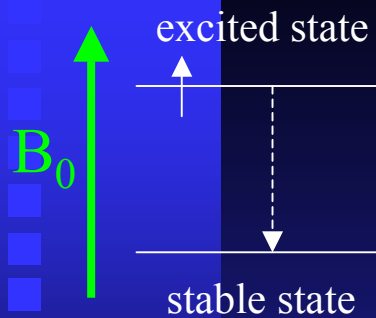
Nuclear spin relaxation



T_2 – spin-spin relaxation time needed to reach the equilibrium inside spin system.

T_1 – spin-lattice relaxation time, at which the spin system comes to equilibrium with the environment releasing its energy to the lattice.

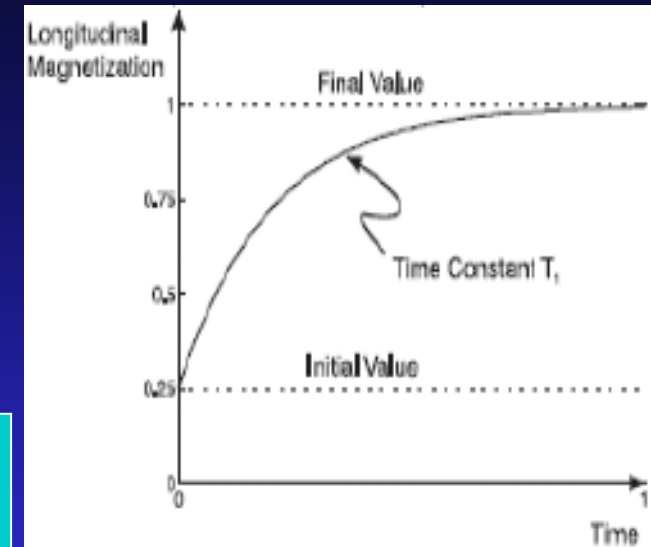
Nuclear spin-lattice relaxation (T_1)



Nuclear spin system
 T_2

T_1

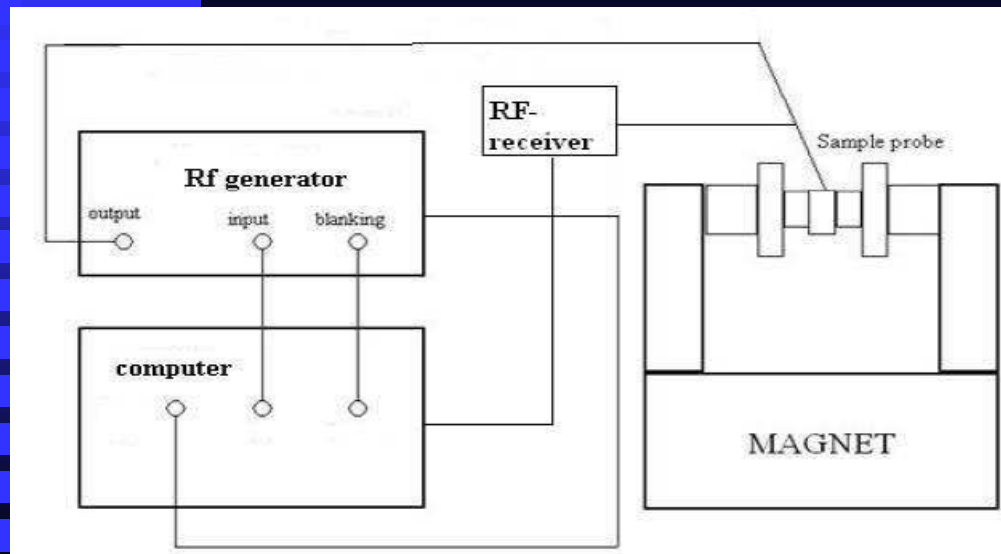
Lattice



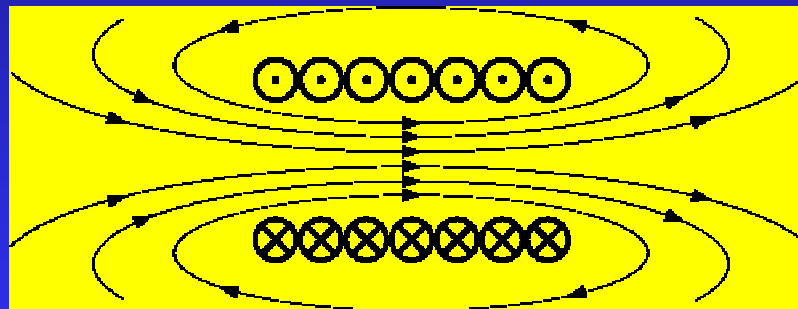
$$M = M_0 [1 - \exp(-t/T_1)]$$

After excitation, spins return to the low-energy state at time T_1 - spin-lattice relaxation time τ . Energy of spin system is released to the environment, or “lattice” (other degrees of freedom), thus spin system comes to equilibrium with the lattice.

NMR spectrometer



Since NMR signal is weak, we use signal acquisition making many scans.



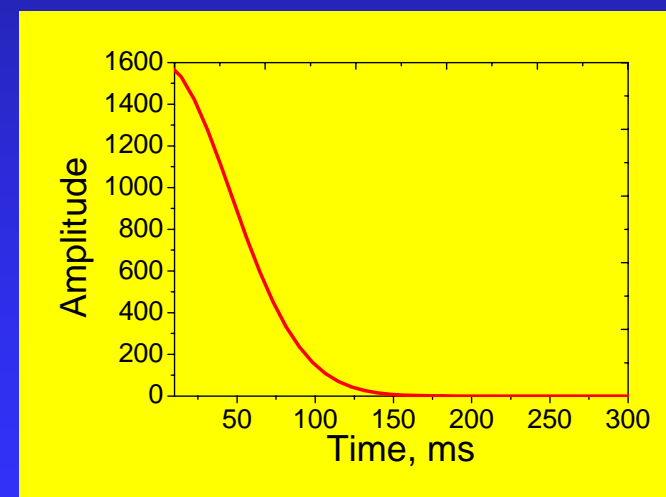
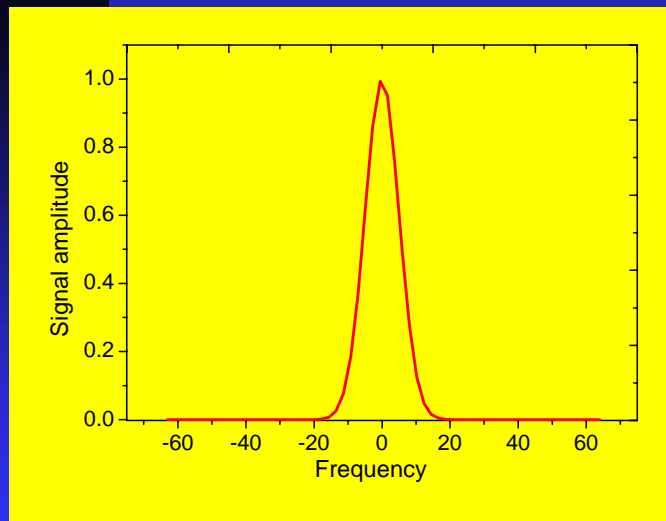
Superconducting magnet in NMR spectrometer.
Magnetic field from 7 to 21 T (70 to 210 kG).

Magnetic field of the Earth is 0.5 G.

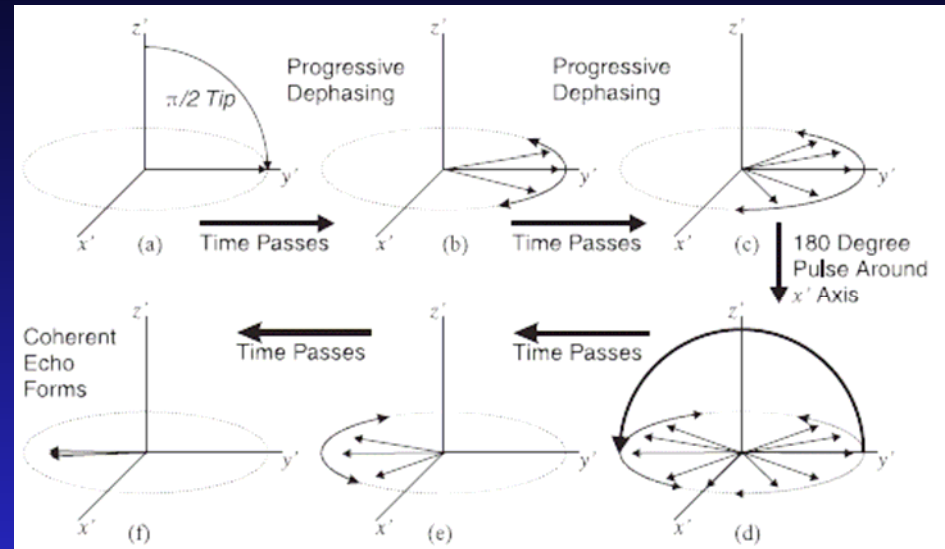
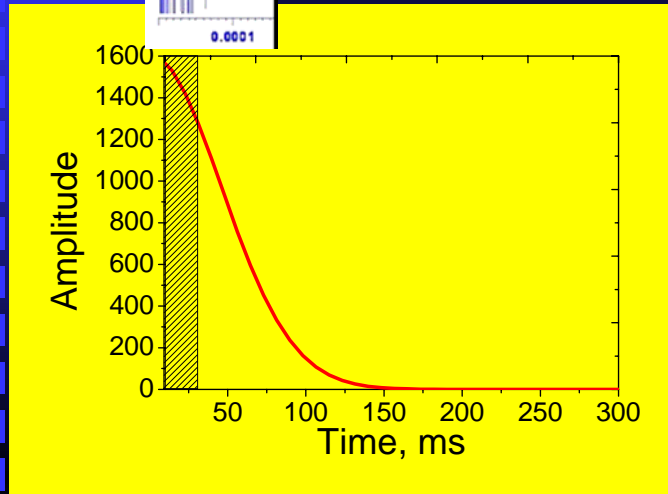
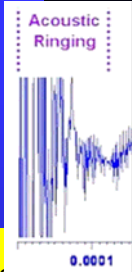


Detection of NMR signals – frequency scan (CW NMR) and pulse NMR

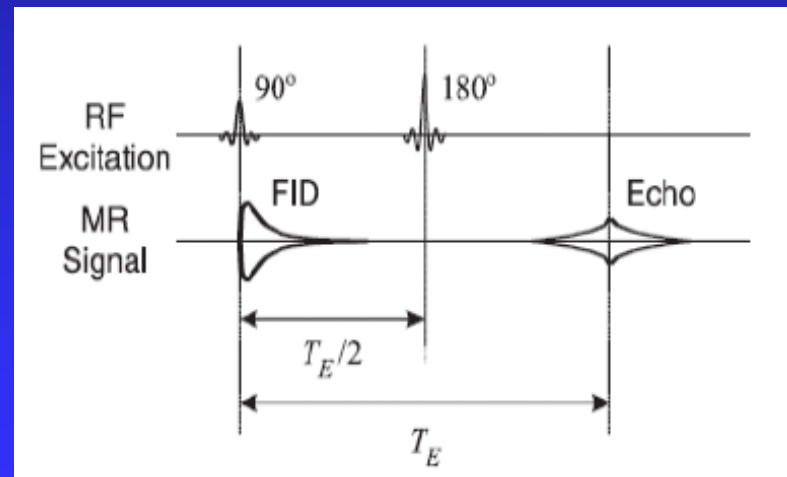
Frequency domain and time domain – two languages of NMR.



Dead time and spin echo technique



When a pulse is applied to NMR probe in magnetic field, the oscillating rf current in the circuit induces mechanical oscillations in metal parts of the probe. This mechanical oscillations in turn generate rf signals detected by the coil. This "acoustic ringing" is seen in the FID and initial part of FID is hidden by the dead time.



2. NMR study of nanocarbon materials

Fullerenes

C₆₀ Fullerene

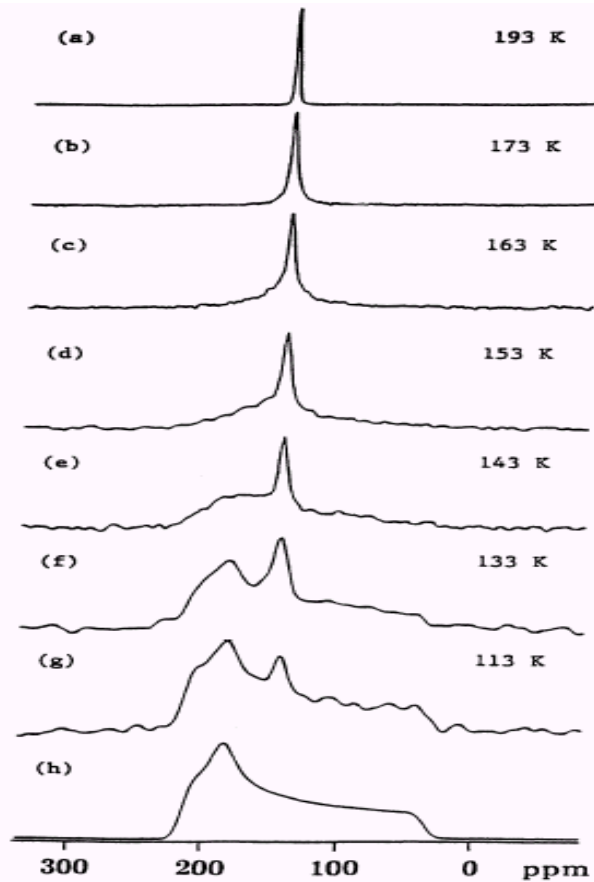
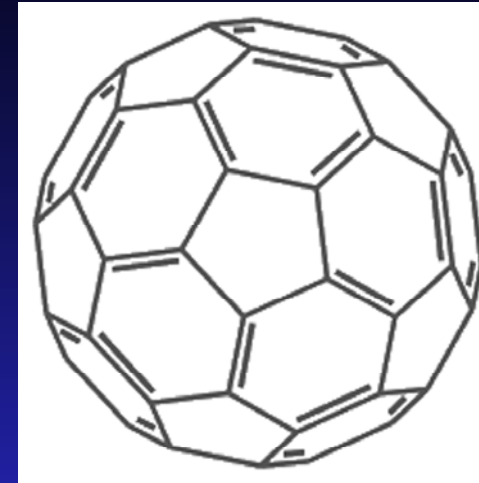


FIG. 2. (a)–(g) ¹³C NMR spectra of solid C₆₀ at indicated temperatures. Frequencies are in ppm with respect to tetramethylsilane. (h) Simulated powder-pattern line shape for rigid molecules with anisotropic ¹³C chemical shielding (principal values $\delta_{11} = 213$ ppm, $\delta_{22} = 182$ ppm, $\delta_{33} = 33$ ppm).

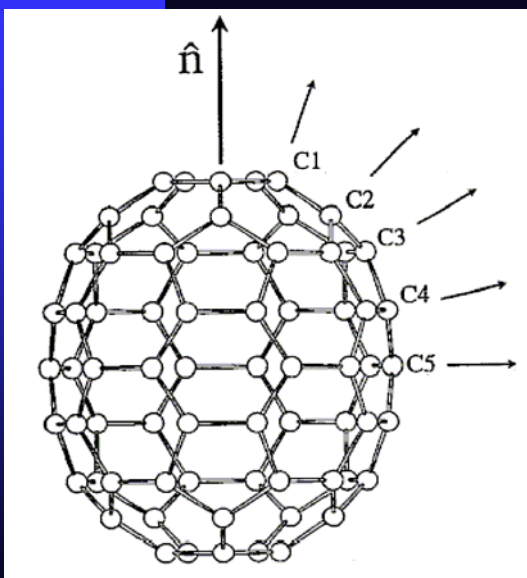
(R. Tycko et al., Phys. Rev. Lett. 67, 1886, 1991).

$\sigma_{iso} = 143$ ppm.

C₆₀ shows non-axially symmetric CS tensor. Why? Three bonds emanating from each carbon atom are a little bit different: two single bonds (pentagonal edges) and one double bond (joining two hexagons). This kills axial symmetry of the carbon site that is reflected in non-axially symmetric CS tensor.

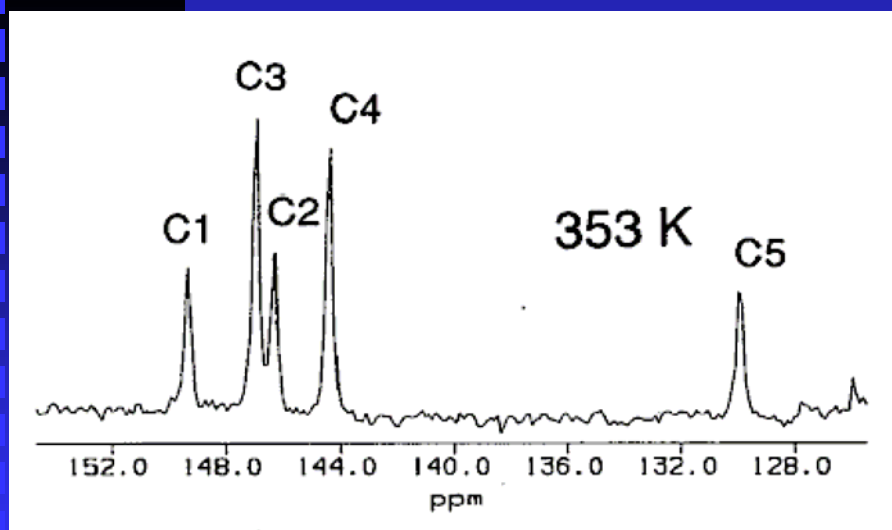
Parameter	Value, Å
C-C bond length on a pentagon	1.46
C-C bond length on a hexagon	1.40

C₇₀ Fullerene



The structure of the C₇₀ molecule, showing the five inequivalent carbon atoms (C1-C5), the fivefold symmetry axis (n), and the directions normal to the molecule's "surface" at each carbon site.

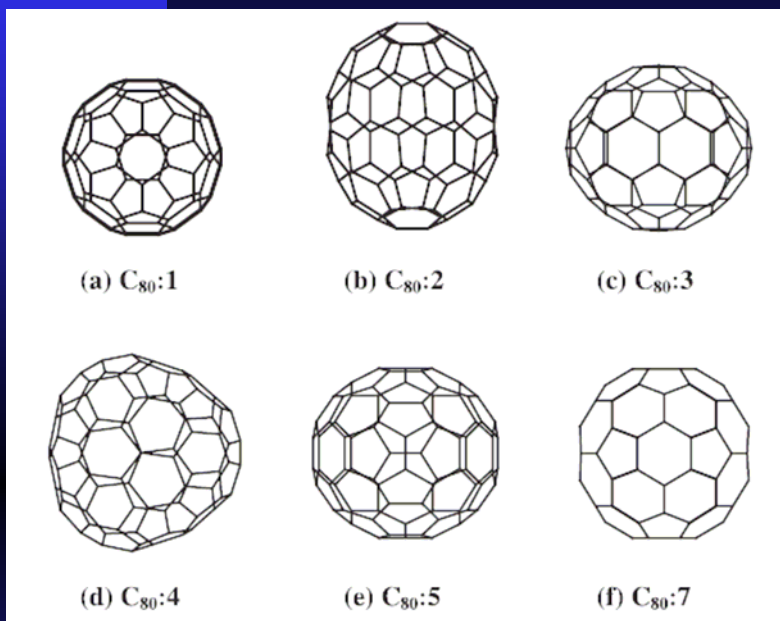
(R. Tycko et. Al., J. Phys. Chem.. **95**, 518 (1991))



¹³C MAS NMR spectrum of solid C₇₀ at T = 353 K at a sample rotation frequency 5 kHz.

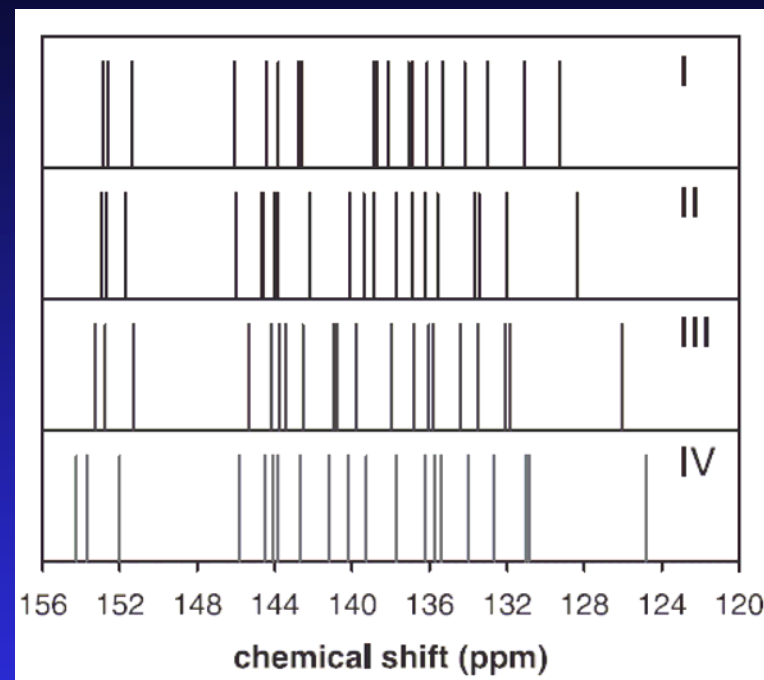
(R. Tycko et. al., J. Chem. Phys. **99**, 7554 (1993))

C₈₀ Fullerene



Six IPR isomers of fullerene C₈₀.

(G. Sun, M. Kertesz, *Chem. Phys. Lett.* 328, 387 (2000)).



¹³C NMR spectra of isomer 2 of C₈₀ by (I) experiment and by (II) B3LYP/6-31G, (III) B3LYP/6-31G*, (IV) B3LYP/6-311G** calculations. Spectra are referenced to C₆₀ at 143.15 ppm.

Static and MAS

NMR spectra in solids

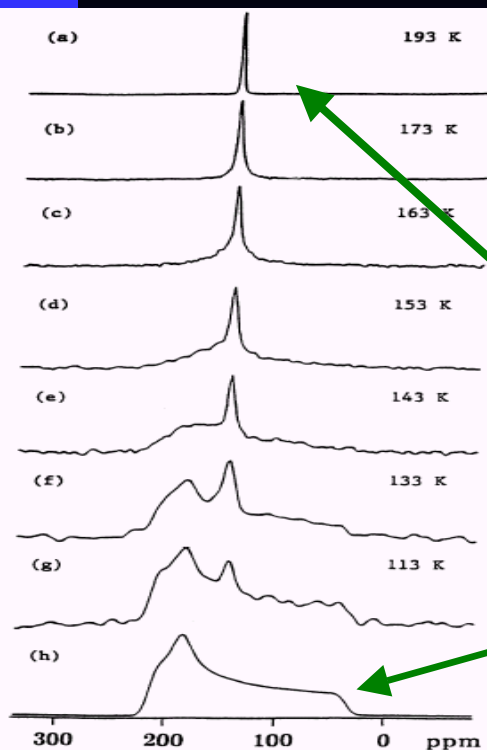


FIG. 2. (a)–(g) ^{13}C NMR spectra of solid C_{60} at indicated temperatures. Frequencies are in ppm with respect to tetramethylsilane. (h) Simulated powder-pattern line shape for rigid molecules with anisotropic ^{13}C chemical shielding (principal values $\delta_{11} = 213$ ppm, $\delta_{22} = 182$ ppm, $\delta_{33} = 33$ ppm).

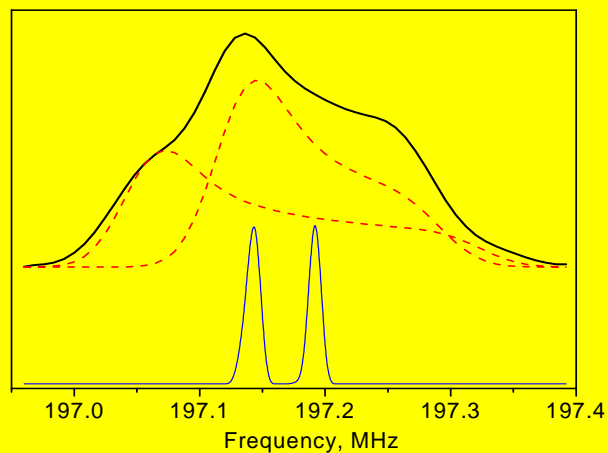
Narrow line

Broad line

Fast rotation of fullerene molecule at RT.

Motional narrowing: Rapid molecular motion yields fluctuations of local fields and averages out anisotropic interactions, resulting in narrow high resolution spectra.

(R. Tycko et al., Phys. Rev. Lett. 67, 1886, 1991)



Solids: often motion does not occur, CSA and dipolar coupling broaden NMR line in powder, resulting in “static” broad-line spectra. If the signals overlap, analysis is sometimes difficult.

Magic Angle Spinning (MAS) of the powder sample:

$$\sigma = \sigma_{\text{iso}} + A(3\cos^2\theta - 1),$$

when $\theta = 54^\circ 44'$ (“magic angle”), $(3\cos^2\theta - 1) = 0$

and the angular dependent term vanishes. It results in well-resolved spectrum and allows accurate determination of chemical shifts.

Doped fullerenes

Solid C_{60} is a semiconductor with an energy gap 1.5 to 1.9 eV. Doping by alkali metals results in essential *electron* charge transfer from metal atom (electron donor) to C_{60} (electron acceptor). K_3C_{60} doped fullerene is metallic compound.

^{13}C NMR signal is shifted by 43 ppm relative to that in undoped C_{60} . This so called Knight shift is due to hyperfine interaction between ^{13}C nuclei and conduction electrons. At that, ^{39}K NMR reveals very small Knight shift, consistent with a model of almost complete charge transfer from K to C_{60} :



Room temperature ^{13}C NMR spectra of C_{60} powder (a) and K_xC_{60} samples with $x=1.5$ (b), $x=2$ (c) and $x=3.1$ (d).

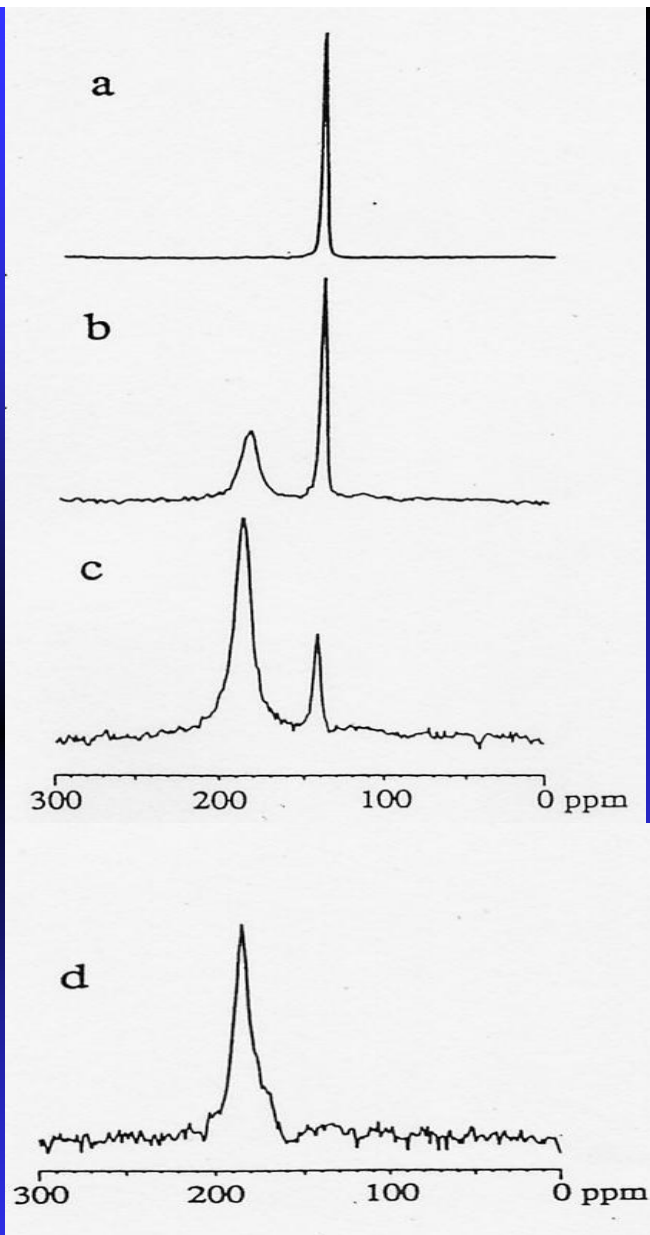
(R. Tycko et al., Science 253, 884, 1991)

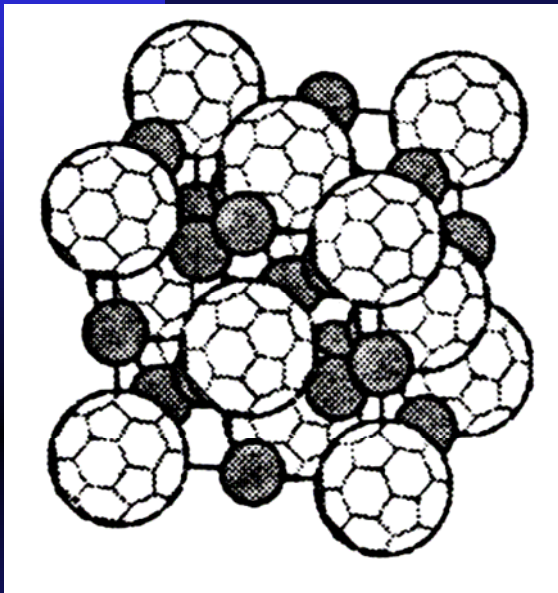
C_{60}
powder

$K_{1.5}C_{60}$

K_2C_{60}

$K_{3.1}C_{60}$

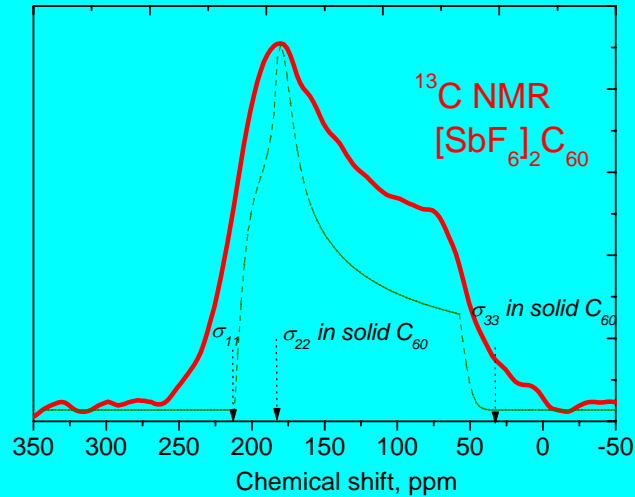




C_{60} molecule is a strong electron acceptor, it is difficult to remove electron from C_{60} . However, doping of C_{60} with very strong acceptor results in $\text{C}_{60}^{2+}(\text{MF}_6)_2^-$ ($\text{M}=\text{As, Sb, P}$), showing removal of 2 electrons from C_{60} .

Acceptor-doped fullerenes are *p*-type semiconductors.

^{13}C NMR in $\text{C}_{60}^{2+}(\text{MF}_6)_2^-$



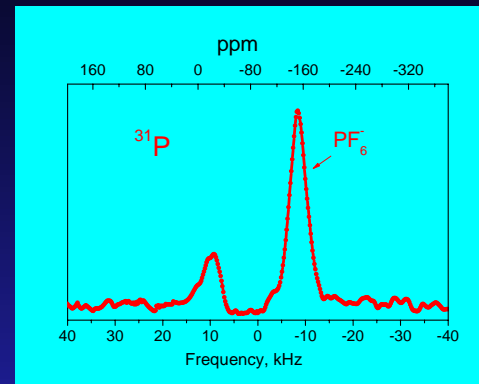
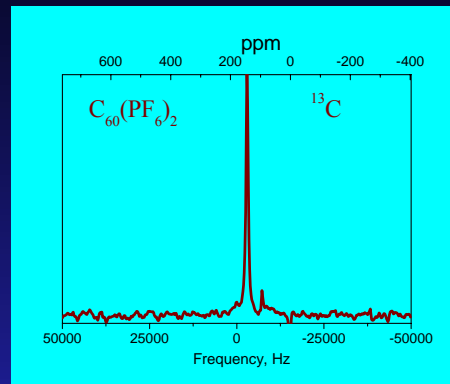
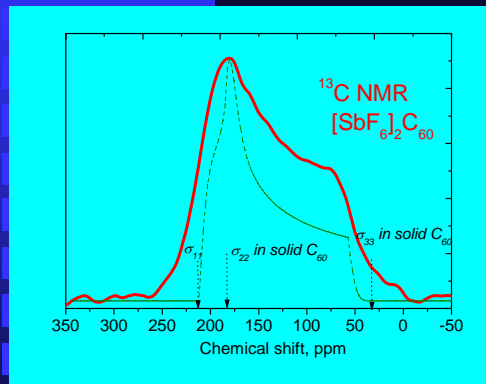
Shift of the center of gravity of ^{13}C NMR line is negligible. Charge transfer results in some reduction in CSA that is detected by NMR, by analogy with GICs that show small variation of CS and larger variation of CSA.

(Panich et al, Solid State Commun. 121, 367, 2002)

	σ_{11} , ppm	σ_{22} , ppm	σ_{33} , ppm	σ_i , ppm	$\Delta\sigma = \sigma_{33} - (\sigma_{11} + \sigma_{22})/2$
“Rigid” C_{60}	213	182	33	143	-165
$(\text{SbF}_6)_2\text{C}_{60}$	209	180	54	148	-141

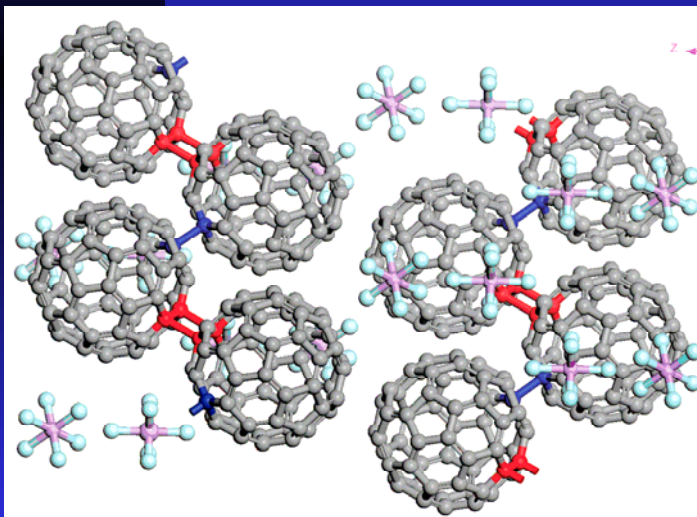
The reason of CSA reduction is occurrence of anisotropic Knight shift that is subtracted from CSA.

^{13}C and ^{19}F NMR and structure of $\text{C}_{60}^{2+}(\text{MF}_6)_2^-$



Broad and narrow lines

(Panich et al, Solid State Commun. 121, 367, 2002), Solid State Commun. 129, 81, 2004)

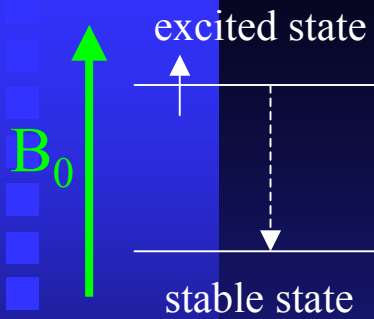


$\text{C}_{60}^{2+}(\text{AsF}_6)_2^-$: AsF₆ rotates, C₆₀ – static.
Polymerization of C₆₀?
1D zigzag polymer structure?

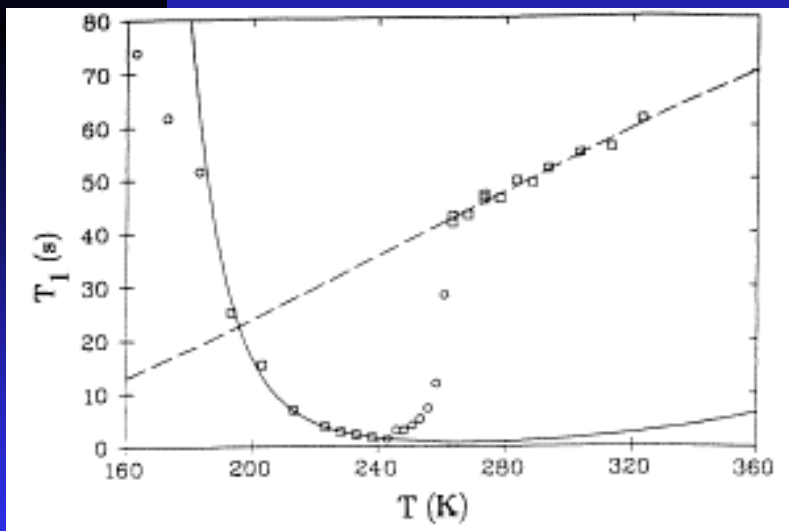
$\text{C}_{60}^{2+}(\text{PF}_6)_2^-$: both PF₆ and C₆₀ rotate

(M. Ricco et al., *J. AM. CHEM. SOC.* **132**, 2064, (2010))

Nuclear spin-lattice relaxation and phase transition in C_{60}



To release energy to lattice, phonons with the Larmor frequency ν_0 are necessary. Therefore T_1 is sensitive to different kinds of lattice dynamics (translations, lattice vibrations, molecular rotations, and other thermal motions and fluctuations in the crystal lattice). Transition is induced rather than spontaneous.



Temperature dependence of the ^{13}C spin-lattice relaxation time T_1 in solid C_{60} .

Phase transition occurs at 260 K.

(R. Tycko et al., Phys. Rev. Lett. 67, 1886, 1991)

Nuclear spin-lattice relaxation and absence of phase transition in C_{60} inside SWCNTs

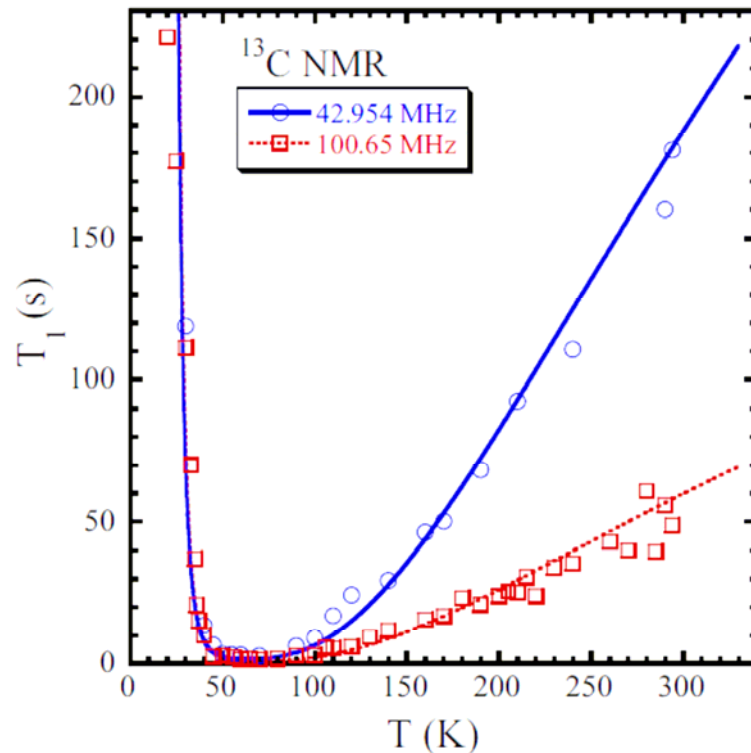
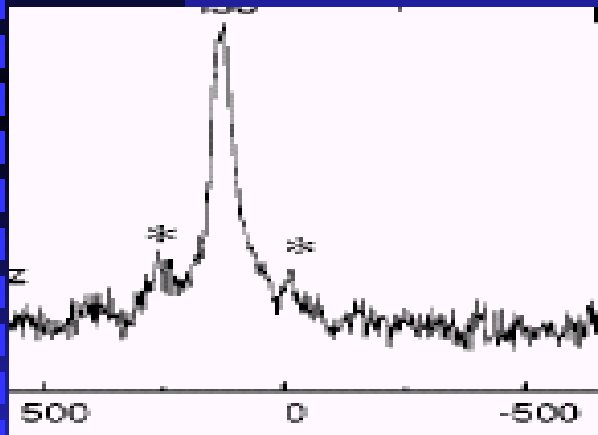
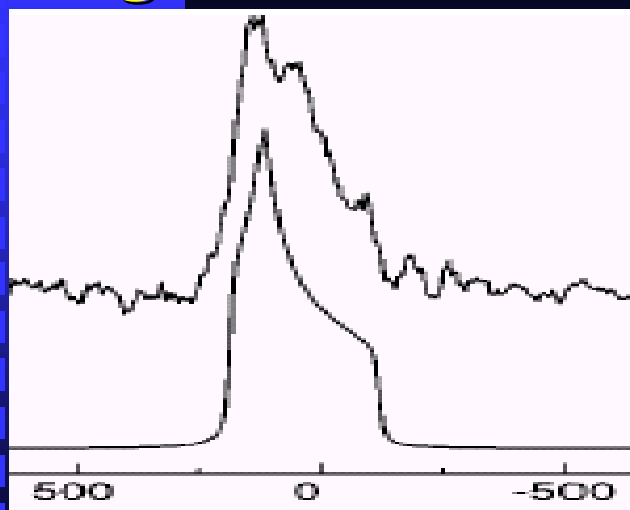


FIG. 3. (Color online) Temperature and frequency dependence of ^{13}C nuclear spin-lattice relaxation time T_1 of encapsulated C_{60} measured at 4.0 T (circles) and 9.4 T (squares). The solid and dotted lines represent the best fits to the T_1 data at 4.0 and 9.4 T, respectively.

(K. Matsuda et al., Phys. Rev. B **77**, 075421, 2008)

Single Wall Carbon Nanotubes. Static and MAS spectra



Top: static ^{13}C NMR spectra (experimental and calculated) of carbon nanotubes. Bottom: high resolution ^{13}C NMR MAS spectrum.

(C. Goze-Bak et al, Phys. Rev. B 63, 100302, 2001)

Articles	σ_{11} , ppm	σ_{22} , ppm	σ_{33} , ppm	σ_{iso} , ppm
H. Peng et al, JACS 2003				121 - 124
C. Goze-Bak et al, PRB 2001	240	171	-36	126
X.-P.Tang et al, Science 2000	195	160	17	124
F. Simon et al, PRL 2005				111 metallic

CS tensor components determined by different authors.

Usually CNT sample is a mixture of metallic and semiconducting nanotubes. Calculation (S. Latil et al, PRL 2001) predicts +11 ppm shift of the signals of metallic CNT relative to that in semiconducting CNT. Two lines have never been observed experimentally. Possible reasons:

- 1) Accuracy is not good enough.
- 2) Distribution of chemical shifts of CNT with different chiralities.
- 3) Calculation is made under some suggestions and are highly approximate.

Single Wall Carbon Nanotubes – spin-lattice relaxation

C. Goze-Bac et al. / Carbon 40 (2002) 1825–1842

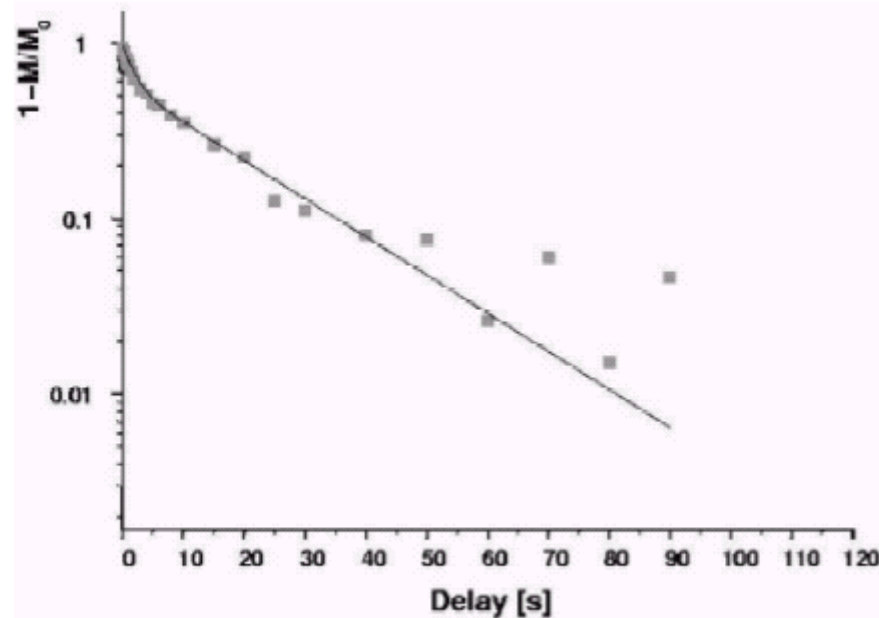


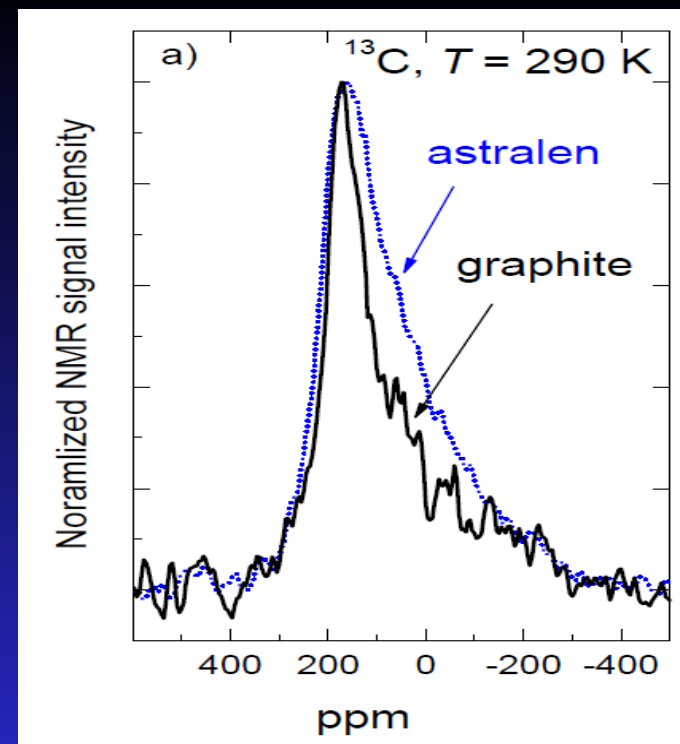
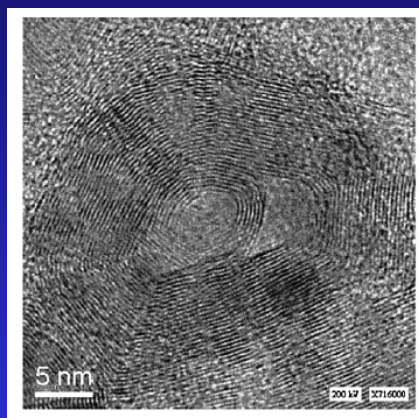
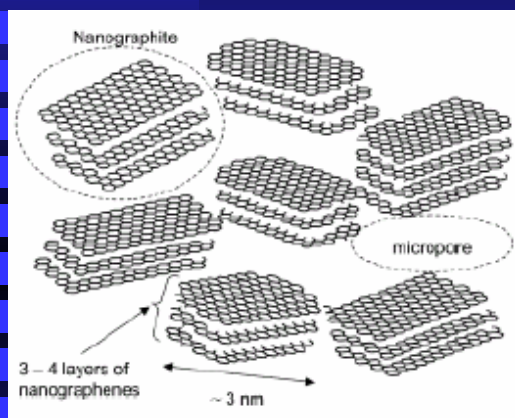
Fig. 5. Magnetization recovery as a function of decay time measured at room temperature.

(C. Goze-Bak et al, *Carbon* 40, 1825, 2002)

Distinguishing between metallic and semiconducting CNTs is possible by measuring spin-lattice relaxation time T_1 that is sensitive to the presence of conduction electrons.

Magnetization recovery is described as a superposition of two components with different $T_1 = 5$ s and 90 s. Fast relaxing component is assigned to metallic CNT, while slow component is assigned to semiconductor CNT.

Nanographite and Large Polyhedral Multi-shell Carbon Nanoparticles (astralen)



Static ^{13}C spectra of graphite and astralen (Shames et al., <http://arxiv.org/abs/0904.2647>, *Nanosci.&Nanotech. Lett.* 3, 41, 2011).

Enoki et al., *Chem. Asian J.*, 4, 796 (2009)

^{13}C NMR spectra of astralen and nanographite are similar to that of graphite. Axially symmetric CS tensor. But if ^{13}C spin-lattice relaxation time in astralen is of the same order that in graphite ($T_1 \sim 110\text{ s}$), $T_1(^{13}\text{C})$ in NG ($T_1 = 3.5\text{ s}$) is much shorter. These findings are attributed to the interaction of nuclear spins with unpaired spins of dangling bonds at the verges of nanographite particle.

Nanodiamonds

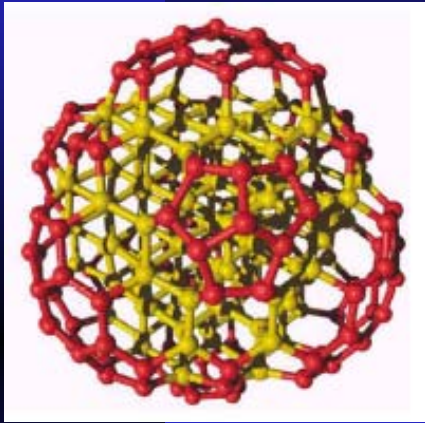
Diamond nanoparticles have risen to the forefront of materials research since they have great potential for a variety of applications:

- additions to lubricants, motor and transformer oils,
- polymer nanocomposites,
- cosmetic products,
- UV-protective coatings,
- protein purification and collection,
- drug delivery (ND is a non-toxic and biocompatible carbon material)
- fluorescence marker applications,
- biosensors, to name just a few.

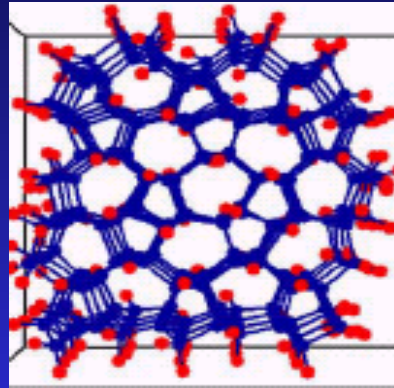
Nanodiamonds (DND) are usually produced in bulk quantities by detonation of carbon-containing explosives and subsequent purification from carbon soot and metallic particles, yielding the DND particles of ~ 4-5 nm in size.

Purified DND

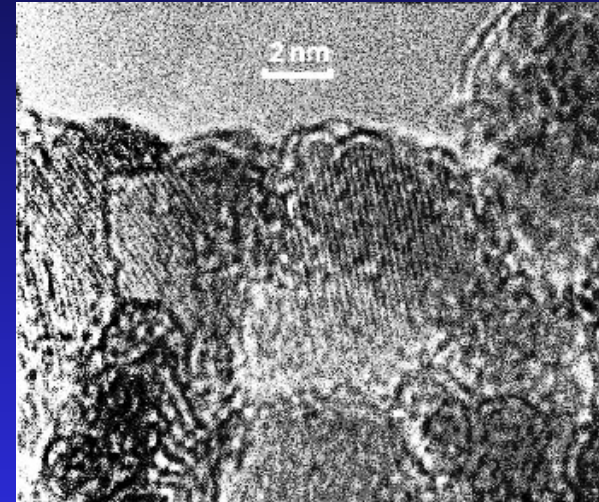
ND particles consist of a mechanically stable and chemically inert diamond core, a shell that covers this core and a chemically active surface with a variety of functional groups.



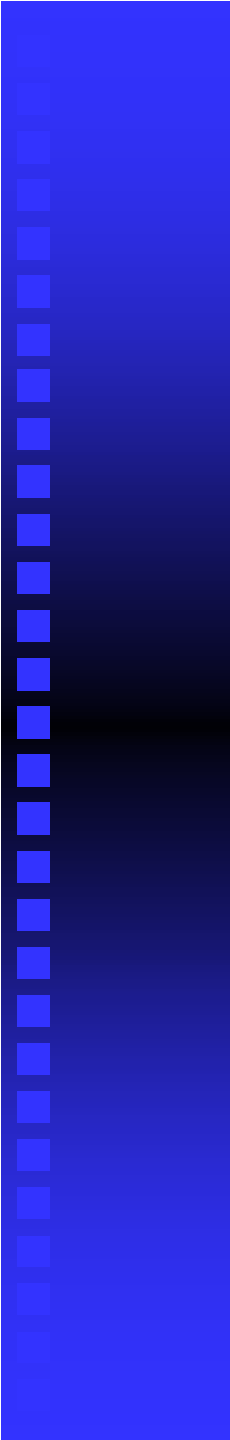
(J. Y. Raty et al. PRL 90,
037401, 2003)



(D.A. Areshkin, O. Shenderova,
Diamond Relat. Mater. 13, 1826,
2004)

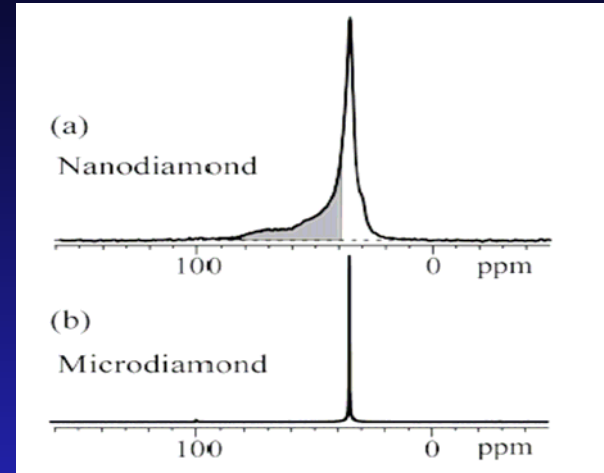
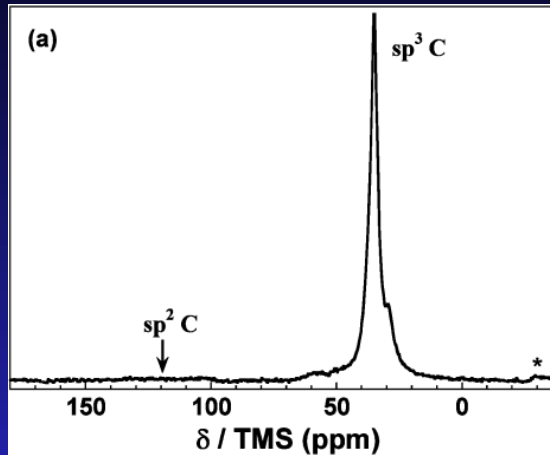
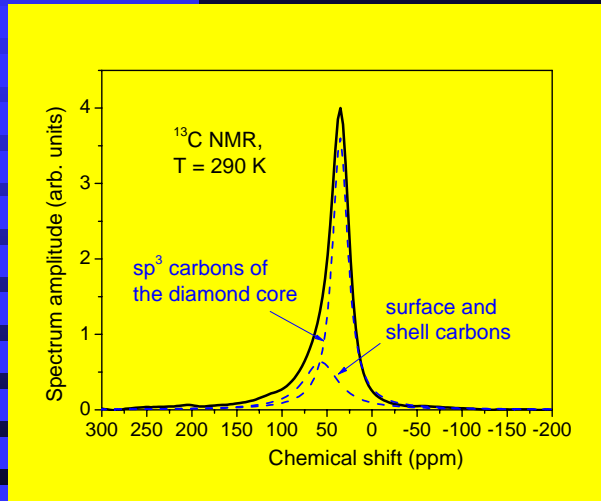


Transmission electron microscopy
(HRTEM) image of DND particles
(Shames et al., J. Phys. Chem. Solids
63, 1993, 2002)



NMR spectra
and
structure
of
purified nanodiamonds

^{13}C NMR: Static and MAS Spectra



(Dubois et al., J. Phys.

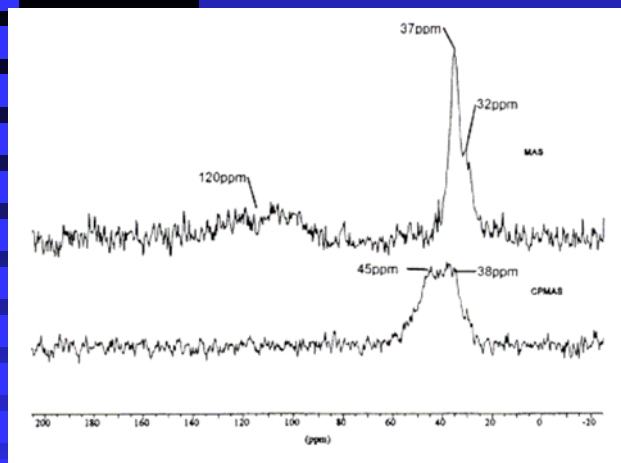
(Fang et al., JACS, 131, 1426, 2009)

Chem. 113, 10371, 2009)

Intense signal at 35 ppm – diamond core

Tail down to 65-85 ppm – shell that covers the core

120 ppm – sp^2 carbons

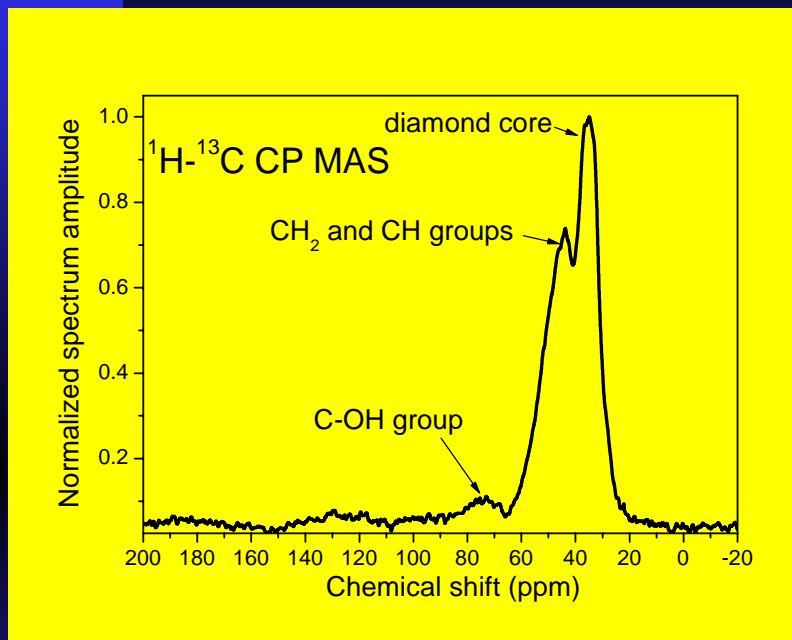


(Donnet et al., C.R. Acad. Sci. Paris Chem., 3, 831, 2001)

NMR measurements show that ND particle consists of a diamond core and a shell that covers this core

35 ppm and shoulder at 32 ppm – perfect and somewhat distorted sp^3 carbon structure in the core

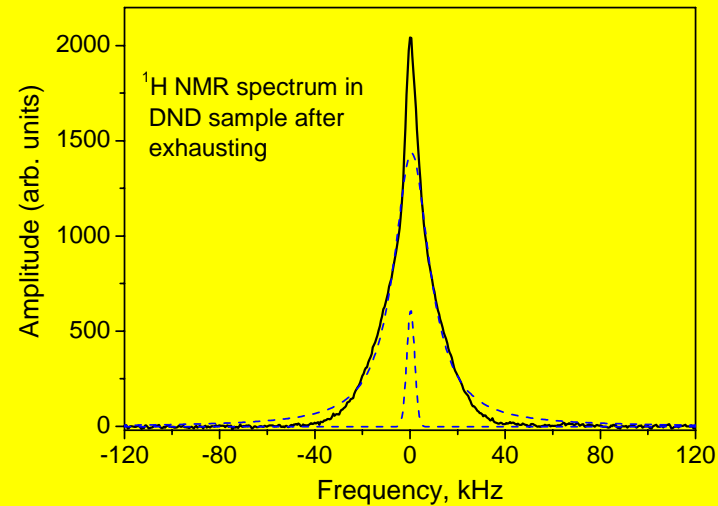
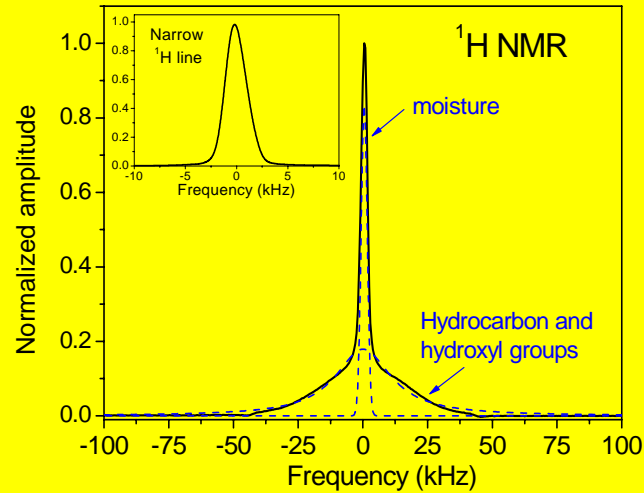
^1H - ^{13}C CPMAS Spectra



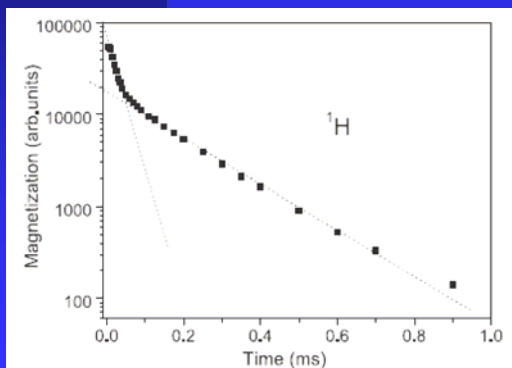
ND surface comprises
hydrocarbon and hydroxyl
groups

(Panich et al., Eur. Phys. J. B 52, 397, 2006)

^1H NMR

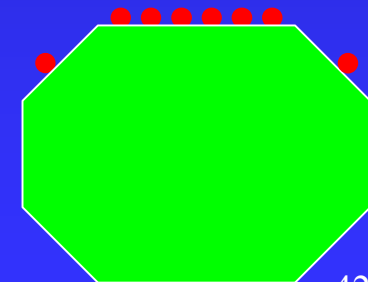


Static room temperature ^1H NMR spectrum of DND sample in $B_0 = 8.0196$ T. Deconvolution: broad component is attributed to rigid hydrocarbon and hydroxyl groups, while the narrow component is mainly assigned to moisture adsorbed onto the DND surface. The latter is significantly reduced after sample exhausting.

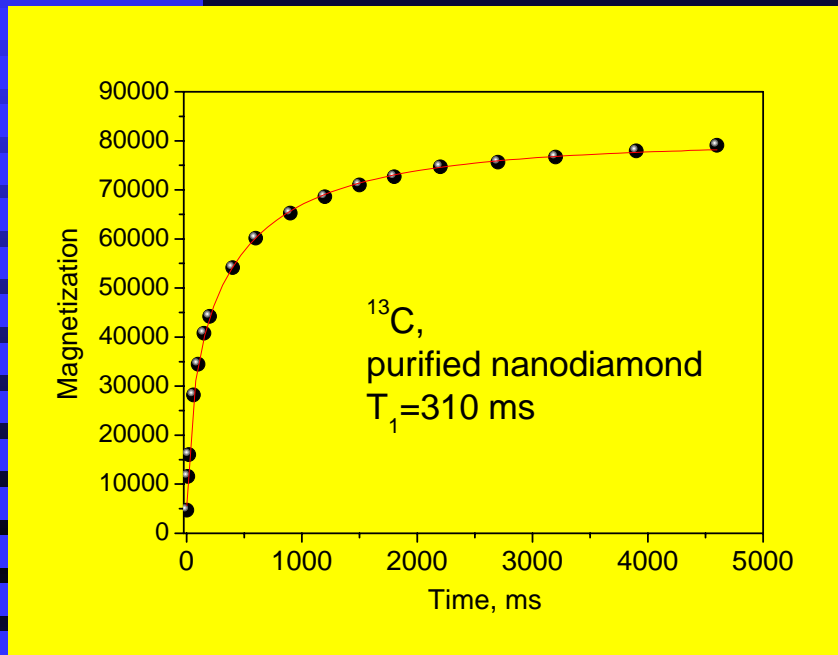


Broad ^{19}F NMR spectrum reflects **strong dipole-dipole interactions among ^1H spins indicating clustering of the hydrogen atoms**. One can assume that the hydrogenated **spots of limited sizes alternate with nearly non-hydrogenated zones in the sample**.

^1H spin echo decay (T_2 measurements) of the DND sample on a semi-logarithmic scale. (Panich et al., Eur. Phys. J. B 52, 397, 2006)



Nuclear Spin-Lattice Relaxation



Natural diamond: $T_1 \sim 10$ h

DND: $T_1 \sim 0.5$ s

Anomalous reduction in ^{13}C spin-lattice relaxation time from several hours/days in natural diamond to hundred *ms* in DND results from the interaction of nuclear spins with electron spins of paramagnetic defects.

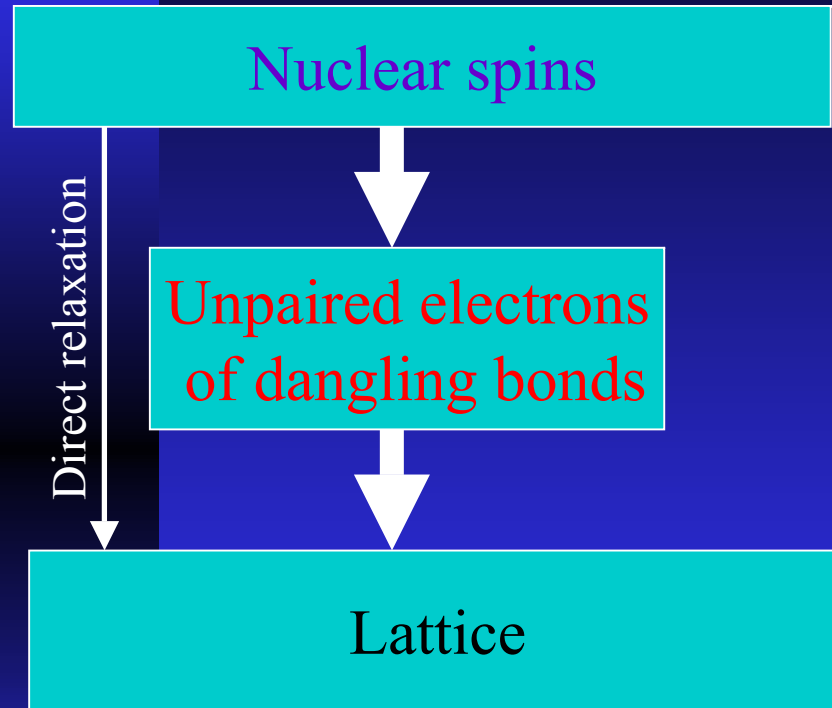
^{13}C magnetization recovery

(T_1 measurements)

of DND sample on a semi-logarithmic scale.

(Panich et al., Eur. Phys. J. B 52, 397, 2006)

Nuclear Spin-Lattice Relaxation via Paramagnetic Centers (unpaired electrons)

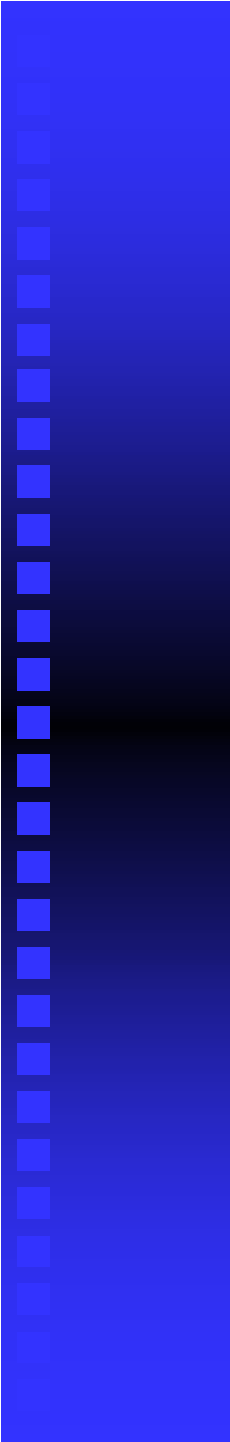


Interaction of nuclear spins with unpaired electron spins opens effective channel for NSLR.

The relaxation via paramagnetic centers is much faster than direct relaxation.

(Panich et al., Appl. Magn. Res. 36, 317, 2009)

EPR: ND particle reveals significant number of paramagnetic defects ($\sim 6 \times 10^{19}$ spin/gram), resulting in fast ^{13}C nuclear spin-lattice relaxation.



**NMR studies
of
Functionalized Nanodiamonds**

Usually we need a compound with specific groups for a specific application.

On-purpose functionalization of the ND surface would lead to fabrication of new materials with controlled chemical, electronic and physical properties.

NDs are extremely attractive objects in science and technology.



Fluorinated nanodiamond (F-DND)

F-DND is a valuable commercial product as its solubility in some polar organic solvents is much higher than that for pristine DND.

Subsequent derivatization of F-DNDs with different functional groups (alkyl-, amino-, and amino acid-nanodiamond derivatives) expands engineering and biomedical applications of DNDs.

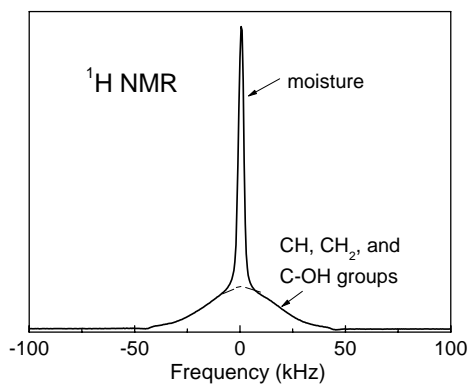
F-DND has been shown to be a wet chemistry precursor for coating glass surfaces with covalently attached diamond particles to be eventually used in optical and biosensor applications.

Fluorinated diamond films showed an improvement in frictional properties and a reduction of the surface energy.

The formation of C–F bonds reduces the dielectric constant (ϵ), implying that F-DNDs may be useful for applications in low- ϵ composites in microelectronics.

Sample Preparation

The fluorination was carried out by introducing fluorine and hydrogen gases in a flow rate of 3:1 over preheated commercial nanodiamond powder at temperatures in the range 150 to 470 °C in a monel reactor for 48 hours.

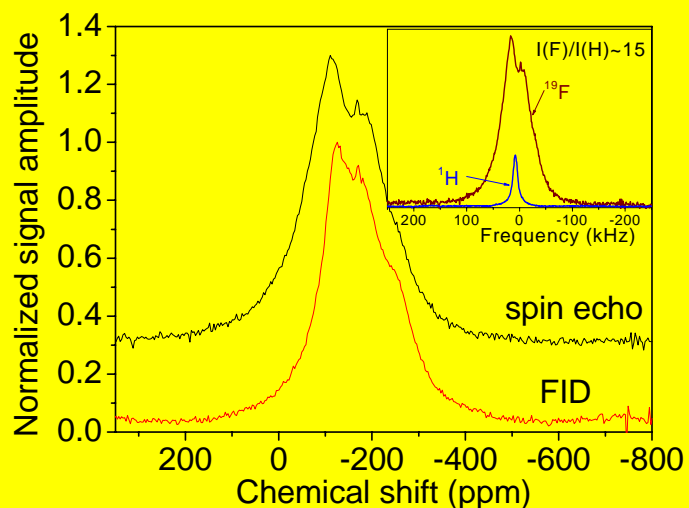


Surface of as-prepared DND is usually hydrogenated

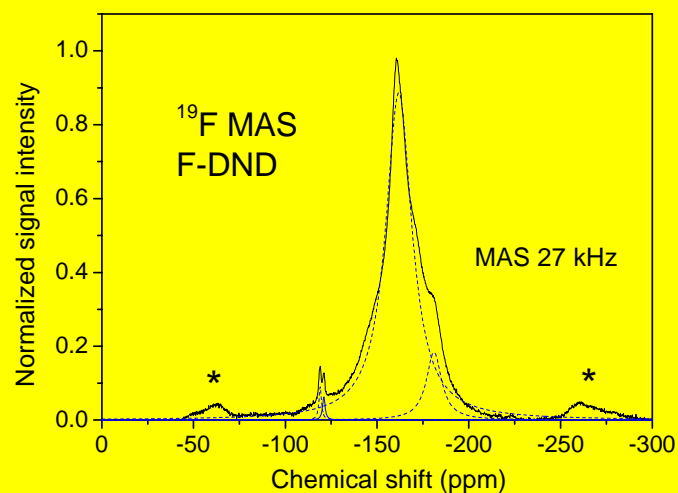
What has been cooked?
What happens with usually hydrogenated nanodiamond surface under fluorination?

Do NMR!

NMR study of structure and bonding in F-DND



Static ^{19}F high field ($B_0 = 8.0196$ T) ^{19}F NMR spectra: strong ^{19}F signal and weak residual proton signal, $I(\text{F})/I(\text{H}) \sim 15$. Hydrocarbon and hydroxyl groups are effectively removed from the DND surface in the process of fluorination and are substituted by the fluorocarbon groups.



^{19}F MAS NMR spectra at $B_0 = 7.04$ T: 3 lines.

Chemical shift $\delta = -120$ ppm: CF_2 groups.

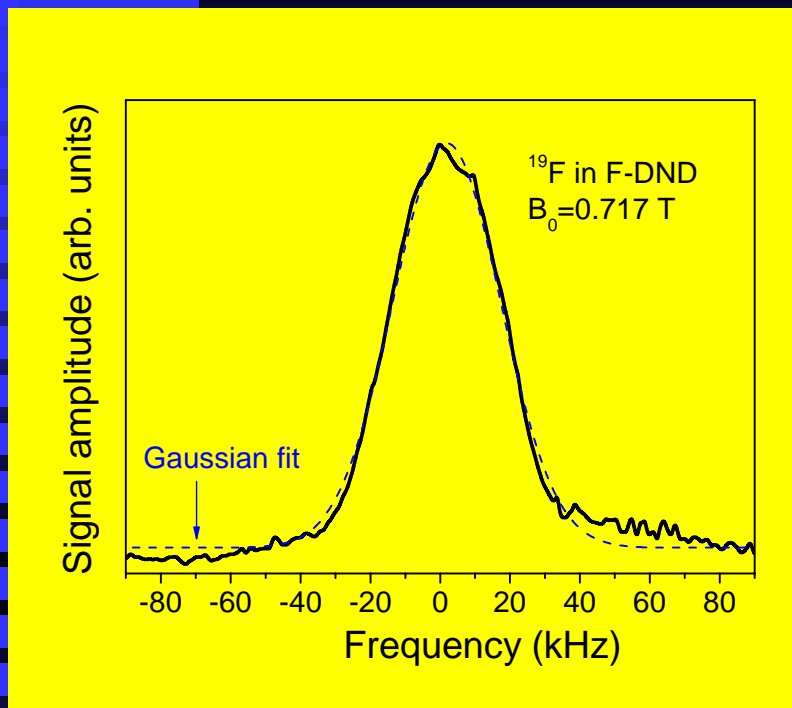
Peaks -162 and -181 ppm - two kinds of C-F groups.

$\delta = -181$ ppm - C-F bonds with sp^3 -hybridization [observed in completely fluorinated graphite $(\text{CF})_n$.]

$\delta = -161$ ppm indicates a more covalent chemical bond characteristic of $(\text{C}_x\text{F})_n$ compounds with $13 > x > 1$: fluorocarbon groups with a distorted of sp^3 -configuration.

CF_2 and two kinds of C-F groups (A. M. Panich *et al.*, *J. Phys. Chem. C* 114, 774, 2010)

Low field ^{19}F NMR spectra



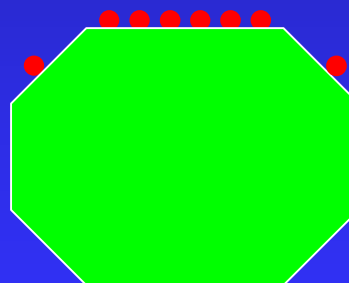
Low magnetic field ($B_0 = 0.717$ T) - CSA contribution to the ^{19}F line shape is small.

Broad ^{19}F NMR spectrum reflects **strong dipole-dipole interactions among ^{19}F spins** indicating clustering of the fluorine atoms.

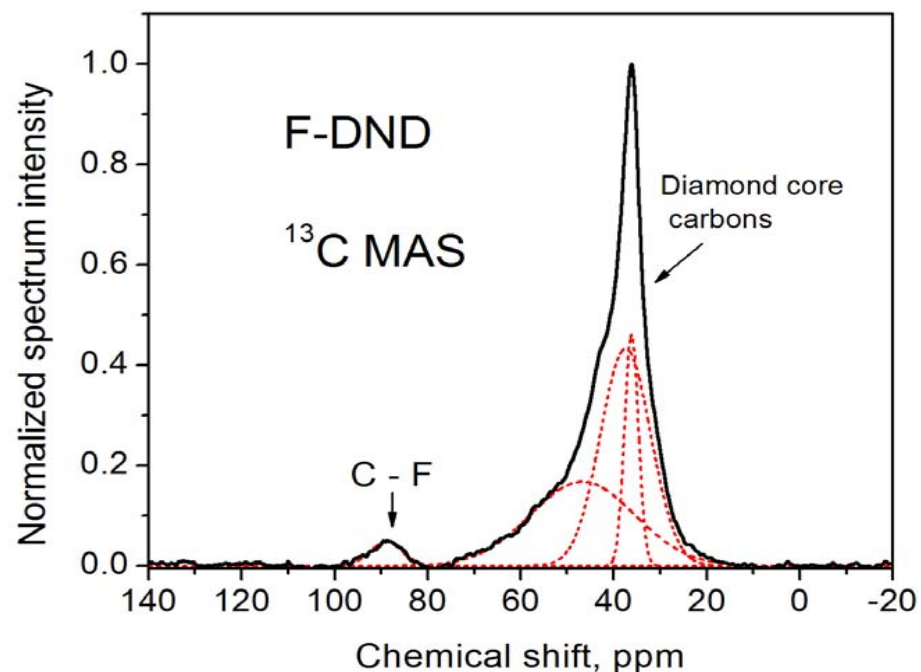
Fluorinated spots of limited sizes alternate with nearly non-fluorinated zones in the sample.

Static ^{19}F NMR spectrum of the fluorinated nanodiamond in $B_0 = 0.717$ T. Gaussian fit is shown by dashed line.

(A. M. Panich *et al.*, *J. Phys. Chem. C* 114, 774, 2010)



^{13}C NMR spectra of F-DND



^{13}C MAS spectrum of F-DND in $B_0 = 14.0954$ T.

^{13}C MAS spectrum:
intense peak $\delta = 36$ ppm
coming from the diamond
core and
peak at 89 ppm from
carbon atoms involved
into covalent C-F bonds.

(A. M. Panich *et al.*, *J. Phys. Chem. C* 114, 774, 2010)

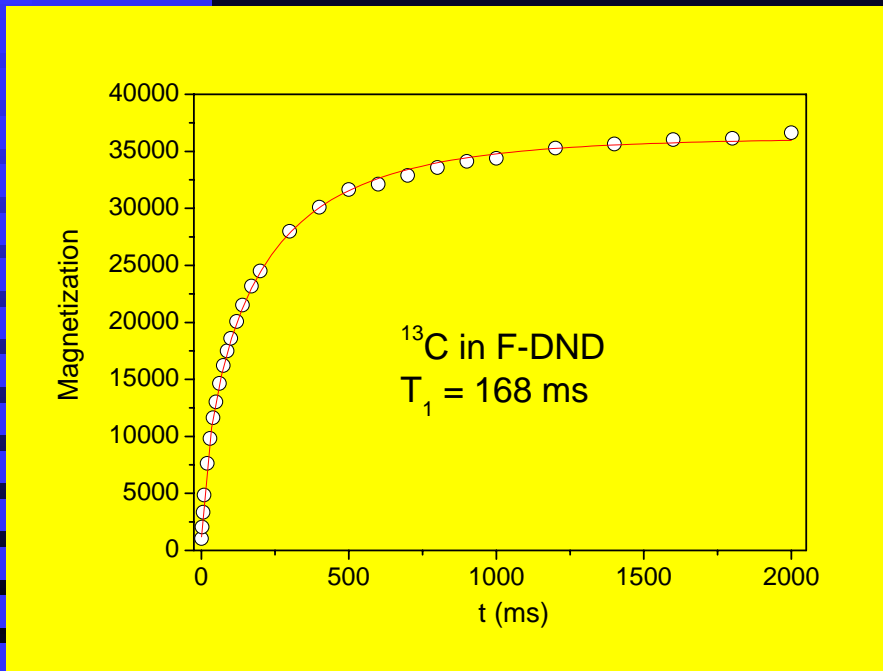
Diamond core peak could be deconvoluted into 3 components - core is not uniform?

Line at 36.1 ppm - the sp^3 -carbons in the perfect part of the diamond core.

Line with $\delta = 37.2$ ppm - somewhat nonequivalent carbon atoms of the diamond core, probably due to some distortion of the tetrahedral sp^3 coordination.

The origin of the broad line showing $\delta = 46.7$ ppm is unclear.

^{13}C spin-lattice relaxation time T_1 of diamond core carbons



Anomalous reduction in the ^{13}C spin-lattice relaxation time from several hours in natural diamond to 168 ms in F-DND resulted from the interaction of nuclear spins with paramagnetic defects.

EPR: $N_s = 1.23 \times 10^{20}$ spin/g is twice larger than that for the initial DND, $N_s = 6.3 \times 10^{19}$ spin/g. These data correlate well with the shortening of the nuclear spin-lattice relaxation time in F-DND ($T_1 = 168$ ms) compared with that in non-fluorinated DND sample (~ 455 ms).

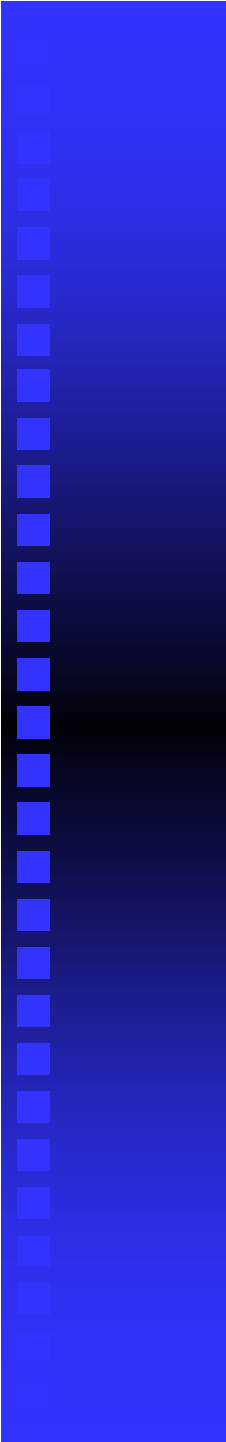
^{13}C magnetization recovery (T_1 measurements) of diamond core carbons in a semi-log scale as a function of recovery time to the power of 0.66.

(A. M. Panich *et al.*, *J. Phys. Chem. C* 114, 774, 2010)

Theory yields $\alpha_{\text{theor}} = 0.5$ and 0.66 for uniform and non-uniform distribution of PM centers.

Experimental value of $\alpha = 0.66$ corresponds to a **non-uniform distribution of the paramagnetic centers**.

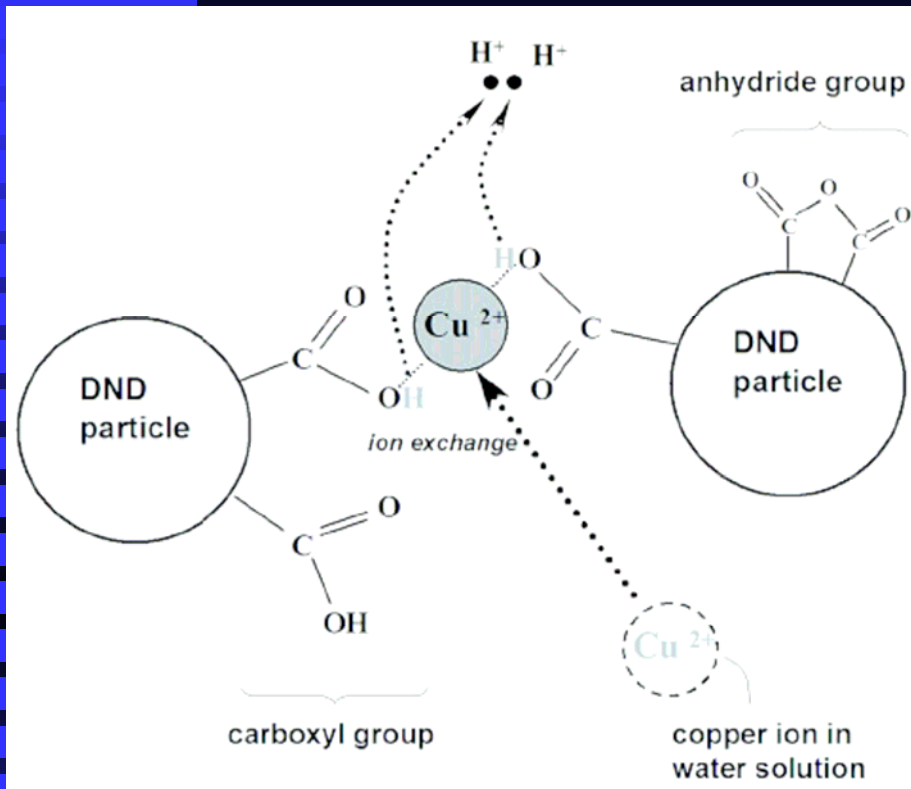
$T_1(^{19}\text{F})$ is very short, 8.9 and 39.6 ms in $B_0 = 0.717$ and 8.0196 T, and $M(t)$ is described by a stretched exponential due to strong interaction of ^{19}F nuclear spins with localized unpaired electrons.



**Diamond nanoparticles
with the surface
decorated by transition metal ions**

for advanced applications

Chemical modification



(Panich et al., Appl. Magn. Res. 36, 317, 2009)

- careful purification of DND in HCl and washing in boiled water;
- EPR and SQUID impurity control;
- intense agitation of mixture of water suspension of DND and water solution of copper acetate to promote chemical modification - ion exchange between Cu^{2+} ion and two protons of the surface carboxyl group
- powder extracted from suspension and dried.

It was expected that divalent copper ion is bound to the nanodiamond surface forming a charge-transfer complex.

Dried Powder Samples

A1 – initial highly purified DND sample

A2 – Cu-DND, 0.06 wt. % Cu

A3 – Cu-DND, 0.6 wt.% Cu

A3-1 – A3 annealed at $T = 550$ °C,

in the hydrogen flow

A3-2 – A3 annealed at $T = 900$ °C,

B3 - Co-DND

B3-1 – B3 annealed at $T = 550$ °C,

in the hydrogen flow

B3-2 – B3 annealed at $T = 900$ °C

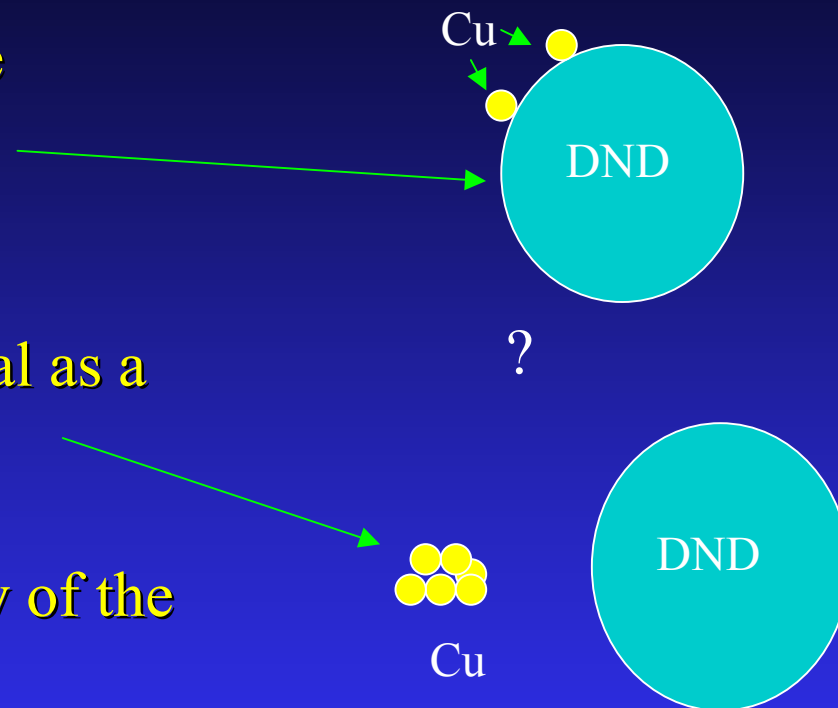
Problem:

Are Cu and Co ions bound to the nanodiamond surface?

Or are they present in the material as a separate phase?

What is the temperature stability of the obtained Cu- and Co-DNDs?

To solve the problem by means of EPR and NMR measurements.

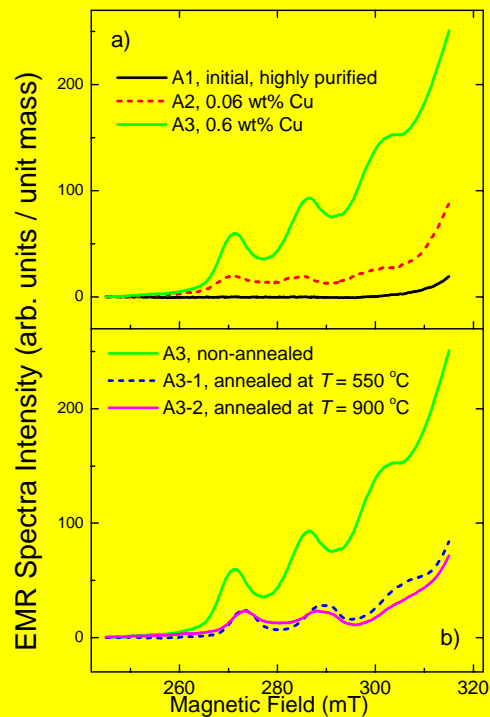
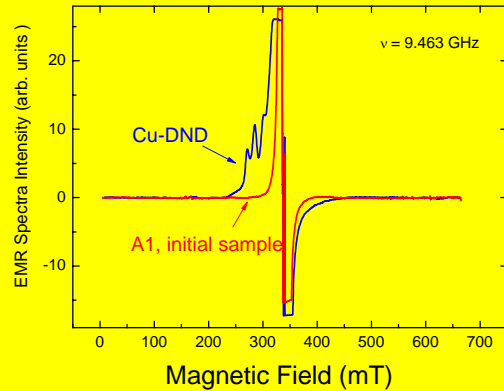


EPR spectra

Initial DND sample shows intensive radical-like singlet originating from unpaired electrons on dangling bonds.

Cu-modified sample –additional signal with pronounced hyperfine structure due to a coupling of electron spin with the spins of $^{63,65}\text{Cu}$ ($I = 3/2$) nuclei. Indicates appearance of magnetically diluted Cu^{2+} ions. Increase in the concentration of copper acetate leads to increase of the corresponding EPR signals. Annealing of the Cu- and Co-DND results in an inverse process, i.e., in a reduction of the signal, indicating that the Cu complexes are destroyed.

We observe Cu^{2+} ions, but where are they located?
On the nanodiamond surface or as a separate phase?
Unambiguous information about the Cu^{2+} and Co^{2+} ions location was received by measurements of ^1H and ^{13}C nuclear spin-lattice relaxation rates R_1 .

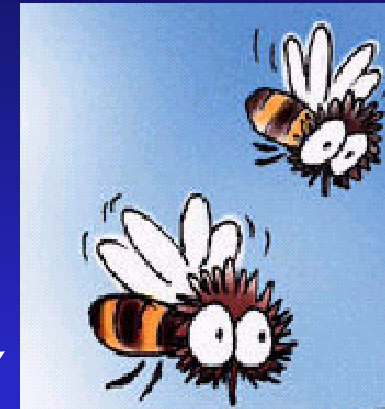


(Panich et al., Appl. Magn. Res. 36, 317, 2009)

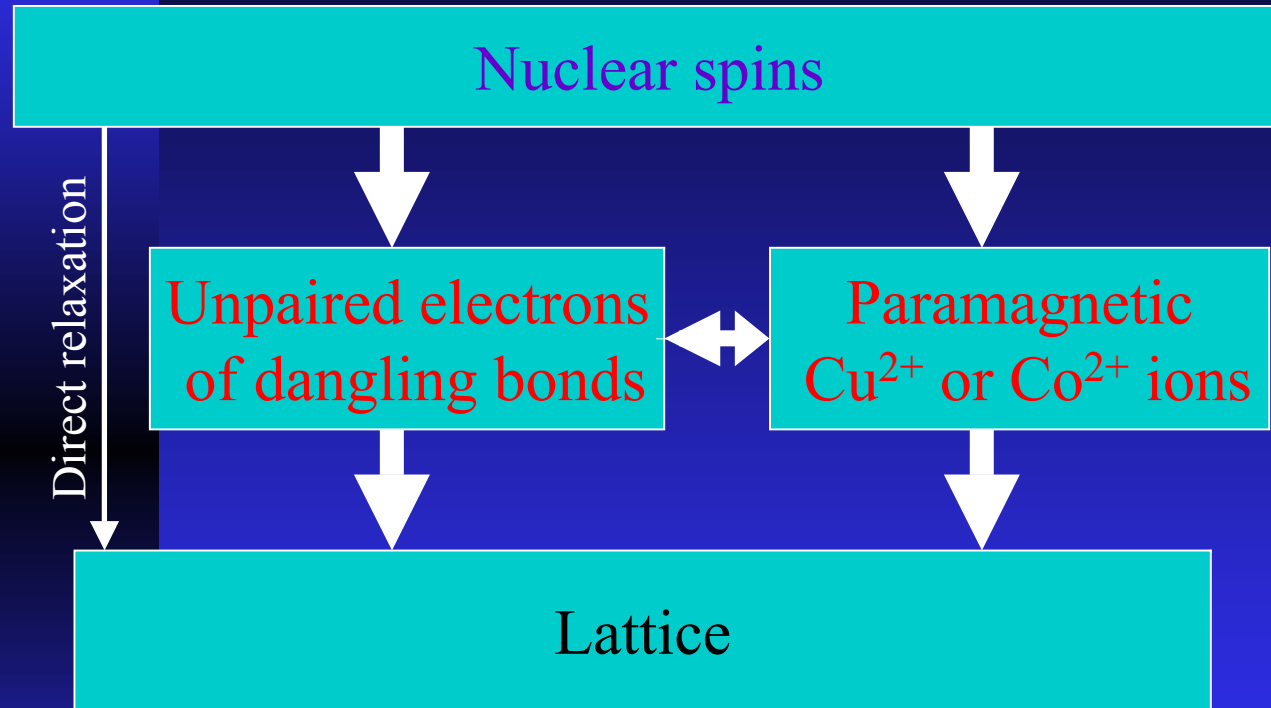


Paramagnetic ions bound to carbon atoms of DND would increase the nuclear spin-lattice relaxation rate,

while if magnetic inclusions are present in a material as a separate phase, this effect is negligible.

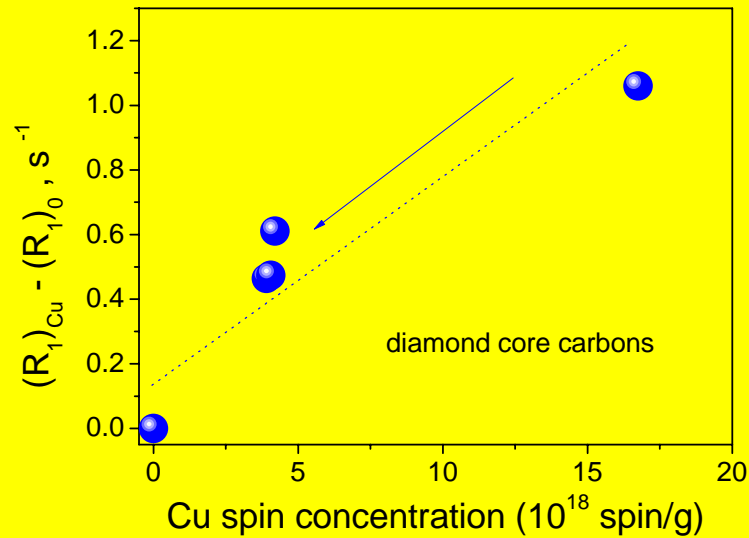


Nuclear spin-lattice relaxation via paramagnetic centers (unpaired electrons)



Spin-lattice relaxation via paramagnetic centers is much faster than the direct relaxation. This fact allows us getting information about the Cu²⁺ and Co²⁺ ion location.

(Panich et al., Appl. Magn. Res. 36, 317, 2009)



Spin-lattice relaxation rate caused by Cu^{2+} ions only against Cu^{2+} content

(other contributions to R_1 are subtracted).

(Panich et al., Appl. Magn. Res. 36, 317, 2009)

^{13}C nuclear relaxation rate R_1 increases with Cu content, showing appearance of paramagnetic Cu^{2+} complexes on the DND surface and their interaction with the carbon nuclear spins.

Annealing of the Cu-modified samples in the hydrogen flow at 550 and 900 °C results in an inverse process, i.e., a reduction of the relaxation rate, indicating that upon annealing these complexes are destroyed.

Co-DND – ^{13}C nuclear spin-lattice relaxation

^{59}Co ($I = 7/2$)

^{13}C spin-lattice relaxation times T_1 in pure and Co-DND samples. T_{11} and T_{12} are attributed to the diamond core and surface carbons.

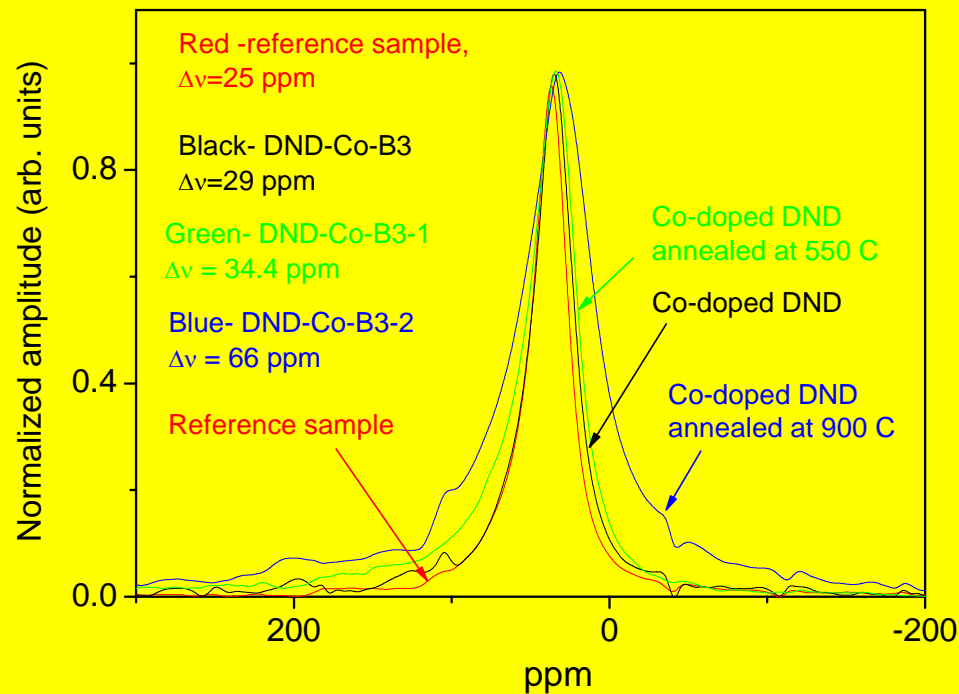
Sample	T_{11} , ms	T_{12} , ms
Reference, B1	615 ± 30	36 ± 4
Co-B3 – Co - modified surface	412 ± 26	22 ± 2
Co-B3-1 – sample B3 annealed at 550 °C	545 ± 20	33 ± 5
Co-B3-2 – sample B3 annealed at 900 °C	575 ± 34	38 ± 6

(Panich et al., Appl. Magn. Res. 36, 317, 2009)

T_1 increases with Co content, while annealing of the Co-DND results in an inverse process, i.e., a reduction of the relaxation rate, indicating that these complexes are destroyed.

Co-DND – ^{13}C spectra

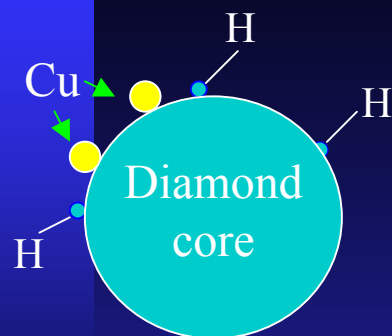
Room temperature static ^{13}C spectra of the reference and Co-doped DND samples at resonance frequency 85.8569 MHz.



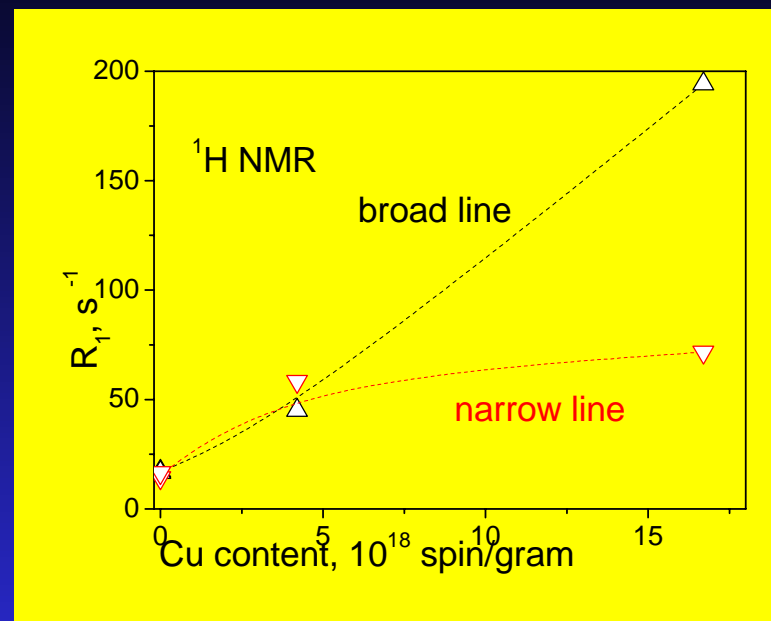
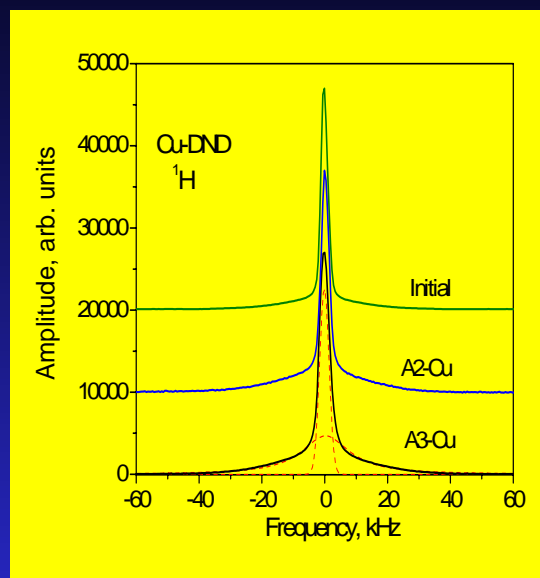
After annealing the Co complexes are destroyed, and metal ions leave the surface and presumably join each other forming nanoclusters. In the case of Co the nanoclusters are ferromagnetic, which results in the noticeable broadening of the ^{13}C NMR lines.

(Panich et al., Appl. Magn. Res. 36, 317, 2009)

^1H NMR in Cu- and Co-DNDs



C-H, CH₂, C-OH
groups



(Panich et al., J.Phys D, 44, 125303, 2011)

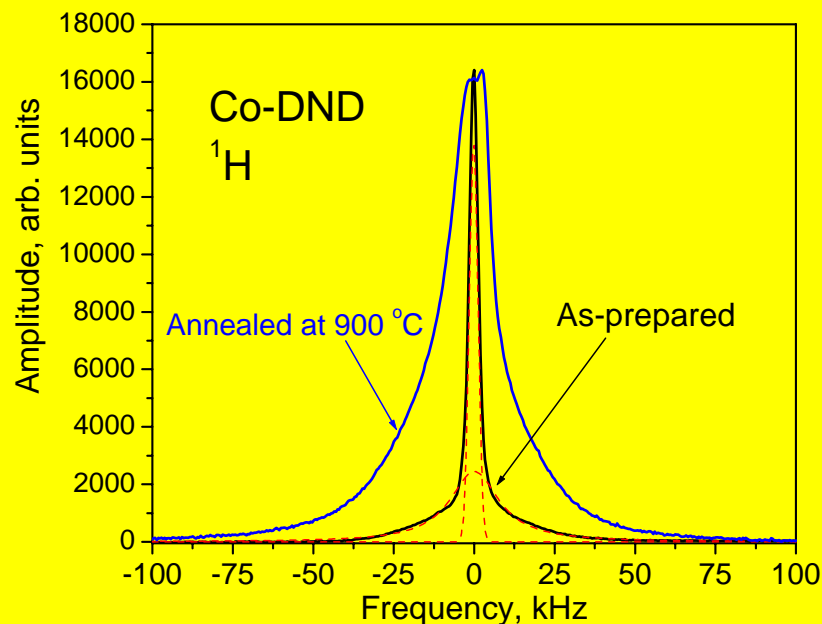
Surface of as-prepared DNDs comprises a number of the hydrocarbon groups.

^1H NMR spectra: broad component is attributed to hydrocarbon groups, while the narrow component is assigned to moisture adsorbed onto the DND surface.

Surface hydrogen atoms should also feel the Cu^{2+} or Co^{2+} ions on the surface due to their interaction with ^1H nuclei.

Increase in $R_1(^1\text{H})$ with increasing Cu content reveals appearance of the paramagnetic Cu^{2+} ions onto the DND surface.

Co-DND – ^1H spectra in as-prepared and annealed samples



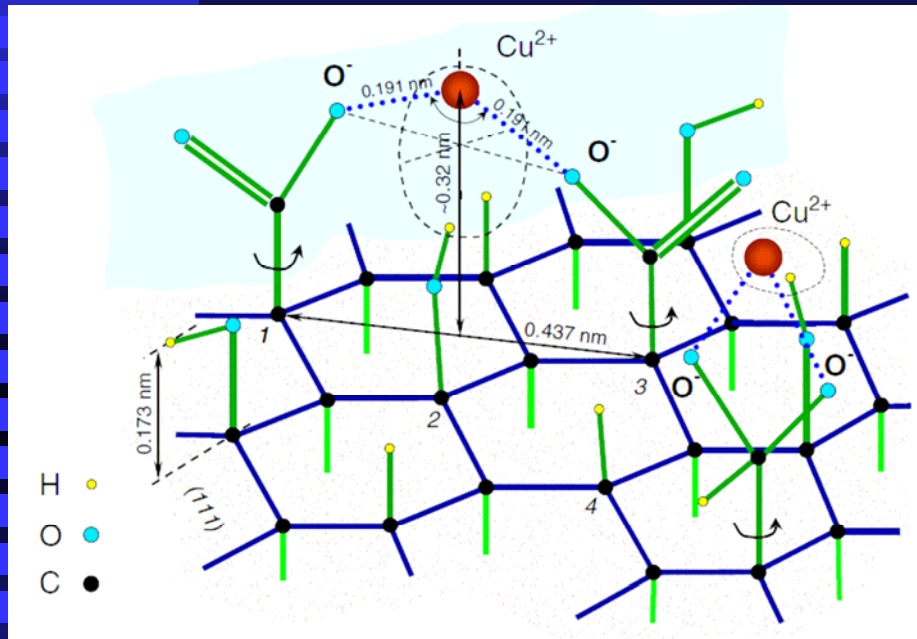
^1H NMR spectra of as-prepared (B3-Co) and annealed at 900 °C (B3-2-Co) nanodiamond samples

(Panich et al., *J.Phys D*, 44, 125303, 2011)

Spectrum of the sample annealed at 900 °C is much broader than that of as-prepared one. Annealing results in cobalt sedimentation and formation of ferromagnetic cobalt (or cobalt carbide) nanoparticles, located separately from the DND particles. Such ferromagnetic inclusions induce additional random magnetic fields at the ^1H nucleus sites, causing the inhomogeneous broadening of the ^1H NMR lines observed in the experiment.

Copper ion configuration on DND surface.

Possible application of Cu-DND



(Panich et al., J. Phys D, 44, 125303, 2011,
drawing by V. Osipov)

Our findings open an opportunity for biomedical applications of modified DND, e.g., for the MRI contrast enhancement, since Cu- and Co-DND particles reduce T_1 of water protons.

(In MRI, ^1H signal intensity is proportional to the relaxation rates of the nuclear spins).

Conclusion:

**NMR is a powerful non-destructive tool in studying
local structure,
electronic structure,
molecular mobility
and paramagnetic defects
in nanocarbon compounds**



"In the Negev will the talents of Jewish science and research be tested..." David Ben-Gurion

Thank you!